UNIVERSIDAD DE CHILE
FACULTAD DE CIENCIAS FÍSICAS Y MATEMÁTICAS
DEPARTAMENTO DE FÍSICA

RECTIFICATION AND CHARACTERIZATION OF DENSE AND HIGHLY CONFINED SUSPENSIONS OF MICRO-SWIMMERS

TESIS PARA OPTAR AL GRADO DE
MAGÍSTER EN CIENCIAS, MENCIÓN FÍSICA

EDGARDO LEOPOLDO ROSAS CÁRCAMO

PROFESORA GUÍA:
MARÍA LUISA CORDERO GARAYAR

MIEMBROS DE LA COMISIÓN:
FRANCISCA GUZMAN LASTRA
TOBIAS WENZEL
NICOLÁS MUJICA FERNÁNDEZ

Este trabajo ha sido parcialmente financiado por Núcleo Milenio Física de la Materia Activa y Fondecyt Regular 1210634

SANTIAGO DE CHILE
2024

Rectificación y caracterización de suspensiones densas y altamente confinadas de micronadadores

Resumen

Las suspensiones densas de micronadadores muestran comportamientos complejos. Un ejemplo de micronadadores son las bacterias flageladas, las cuales generan un flujo en el medio circundante. Este flujo es capaz de mover objetos situados dentro o fuera de la suspensión, y bajo un confinamiento esférico, la suspensión es capaz de propulsarse a sí misma.

En esta tesis se realizaron experimentos exploratorios de los flujos y movimientos inducidos por suspensiones de alta densidad de bacterias en tres configuraciones. La motivación es caracterizar el movimiento generado por un baño de bacterias y extraer trabajo útil de él. Dos tipos de confinamientos fueron estudiados, un confinamiento plano cuasi-bidimensional llamado alfombras activas, y un confinamiento esférico llamado gotas activas. Dependiendo de la configuración, las gotas activas son capaces de auto-propulsarse, en cuyo caso las llamamos motores bacterianos traslacionales (TBM por su sigla en inglés).

La primera parte de esta tesis se enfoca en alfombras activas de bacterias *Escherichia coli*. Primero, se explica un nuevo método para generar este tipo de sistemas. Luego estudiamos la propulsión de partículas pasivas situadas sobre las carpetas activas, generada por las bacterias que se encuentran en la carpeta activa. Se obtuvo el desplazamiento cuadrático medio (MSD por su sigla en inglés) para las partículas pasivas, mostrando un régimen balístico a tiempos cortos, y uno difusivo a tiempos largos. Usando un modelo teórico para ajustar las curvas de MSD hemos caracterizado la velocidad de persistencia v y el tiempo de persistencia τ en el régimen balístico, y el coeficiente de difusión D para el régimen difusivo, todos como función del tamaño de la partícula. Hemos observado que v y D crecen con el tamaño de la partícula, mientras que τ no tiene una dependencia clara con el tamaño de la partícula.

La segunda parte es sobre las gotas activas. Se estudió el flujo generado dentro de las gotas de *E. coli* y *Bacillus subtilis* usando la técnica de descomposición ortogonal propia. Se muestra que en ambos casos la geometría juega un rol importante en los patrones de flujo debido a la existencia de modos de borde. Mas aún, se observó que la actividad de las *B. subtilis* tiende a concentrarse en los bordes de las gotas, a diferencia de las *E. coli*. Esto podría deberse a la diferente geometría de los cuerpos de ambas especies de bacterias.

La última parte es sobre TBMs. Estudiando su MSD hemos observado nuevamente un régimen balístico a tiempos cortos y uno difusivo a tiempos largos. Obtuvimos la velocidad de persistencia y el tiempo característico para el régimen balístico y el coeficiente de difusión a tiempos largos como función del tamaño del TBM. Además, intentamos la rectificación de TBMs usando dos micro-dispositivos de fabricación propia. Los protocolos de fabricación de cada micro-dispositivo y su efectividad en la rectificación han sido reportados.

Abstract

Dense suspensions of micro-swimmers show exotic behaviors. Micro-swimmers, such as flagellated bacteria, generate flows within the surrounding medium, which generate movement on objects located inside or outside the suspension. When the suspension is confined inside drops immersed in oil, the flows generated by the micro-swimmers can propel the whole drop.

In this thesis, an experimental exploratory study of the flows and movements induced by high-density suspensions of bacteria in different confined configurations was carried out. The motivation of these studies is to characterize the motion generated by a dense bath of swimming bacteria and extract useful work from it. Two confinements were studied in this thesis, a flat quasi-two-dimensional confinement called active carpet, and a spherical confinement called active droplets. Depending on the configuration, the active droplets are capable of self-propulsion, in which case we call them translational bacterial motors (TBM).

The first part of this thesis focuses on the results obtained for active carpets of *Escherichia coli*. First, a new way to generate this type of systems is explained. Then, we study the propulsion of passive particles laying on top of the active carpets, by the micro-swimmers in the active carpet. The mean square displacement (MSD) of the passive particles was measured, showing a ballistic regime at short times and a diffusive one at long times. Using a theoretical model to fit the MSD curves, we characterize the persistence velocity v and persistence time τ for the ballistic regime and the diffusion coefficient D at long times as a function of particle size. We observed that v and D increase with particle size, while τ has no clear dependence on particle size.

The second part is about active droplets. The flow generated inside active droplets formed by *E. coli* and *Bacillus subtilis* was studied using the proper orthogonal decomposition technique. This study shows that in both cases the geometry plays an important role in the flow pattern due to the existence of edge modes. Furthermore, it was observed that the activity of *B. subtilis* tends to be concentrated at the edges of the drops, while that of *E. coli* droplets is homogeneous. This could be due to the different geometry of the two bacterial strains, with *B. subtilis* having a larger body size with respect to its width than *E. coli*.

The last part is about TBMs. By studying their MSD, we observed again a ballistic regime at short times and a diffusive one at long times. We obtained the persistence velocity and the time scale for the ballistic regime and the diffusion coefficient at long times as a function of the TBM size. In addition, we have attempted the rectification of TBMs using two micro-devices of our own fabrication. The fabrication protocols of each micro-device and their effectiveness in rectification are presented in detail.

A los profesores , que traspasan de manera apasionada sus mas valiosos conocimientos.

Acknowledgments

Esta tesis de magister es el fruto de 3 años de trabajo. Fue un viaje con muchos altibajos, que estuvo lleno de aprendizajes y de crecimiento. Es justo agradecer a todos y todas quienes estuvieron presente y que hicieron de este viaje una experiencia agradable, que estuvieron allí para apoyarme, y que de alguna u otra manera formaron parte de mi vida durante el transcurso de este trabajo.

En primer lugar me gustaría agradecer a mis padres: Erica y Edgardo, por apoyarme de manera incondicional a lograr mis metas y objetivos. Sentir el soporte que me han brindado ha sido muy importante para mi.

También quiero agradecer a María Luisa por ser mi mentora en esta etapa de mi carrera. Gracias por confiar en mi, por brindarme libertad en muchas cosas, y por todos los consejos para presentar adecuadamente mis resultados y para mejorar mi escritura científica.

Quiero agradecer a mis amigos Gabo, Nava y JP por los muchos buenos momentos que pasamos juntos, los memes, las risas y los momentos de distensión, las conversaciones profundas y estimulantes, y por permitirme encontrar en ustedes un lugar seguro en el cual me he sentido acogido y entendido durante el transcurso de esta tesis.

Agradezco la presencia de Fer, por estar en presente en el último período de este trabajo, por brindarme un soporte emocional muy importante para seguir adelante. También por las infinitas alegrías y risas que compartimos, las conversaciones estimulantes y profundas, y las valiosas discusiones y consejos que me brindaste.

Quiero agradecer a los miembros del Núcleo Milenio Física de la Materia Activa por generar un espacio muy enriquecedor, tanto del punto de vista académico como desde el punto de vista humano. A los académicos María Luisa, Rodrigo, Francisca e Ignacio. A los estudiantes, Paulo, Aguayo, Chaivo, Rojo, Fer, JP, Pablete. A los post-doc Kevin y Viviana. Discutir de ciencia con ustedes siempre fue un placer. El ambiente siempre fue muy estimulante, y muy seguro para el aprendizaje.

Me gustaría dar mención a Rojo quién me enseño a hacer mi primer experimento en el laboratorio, fue muy emocionante para mi. También a Cristian que me traspasó mucho de su conocimiento y experiencia. Aprendí mucho de ambos.

Gracias a mis compañeros y amigos del tercer piso del DFI: Al Luquitas, Phalo, Colipí, Rojo, Chaivo, Gaga, Clau, Gabo, JP y Nava. Fueron muy entretenidos y chistosos los almuerzos que compartimos juntos, gracias por el ambiente tan agradable.

Por último, no me gustaría dejar en el olvido a quienes desde el colegio me alentaron a seguir cuestionándome y haciéndome preguntas, a mis queridos profesores que generaron un ambiente muy estimulante para el aprendizaje. Gracias Antonio, Nancy, Edgardo, Juan, Carlos, Laura, Vilma.

Table of Content

List of Tables

List of Figures

Chapter 1

Introduction

1.1 Active Matter

Biophysics is an interdisciplinary field that employs principles and methods from physics to investigate and understand biological systems at the molecular, cellular, and organismal levels. It seeks to apply quantitative techniques to analyze biological phenomena, elucidating the underlying physical principles that govern biological processes.

Active matter is a sub-field of biophysics that aims to study particles that can convert their internal energy into motion, often referred to as active particles [Das et al., 2020]. Most examples of active matter are biological in nature, found in contexts where there are variable numbers of active particles and exist at a variety of length scales. At the micro-scale, examples of active matter are swarms of bacteria, bacterial suspensions, and cellular tissues. In contrast, flocks of birds, schools of fish, and even a crowd of people are examples of active matter at the macro-scale (see Fig 1.1). There are, however, notable examples of non-biological systems that exhibit behaviour that is remarkably similar to that of active matter. Examples of that include active particles such as bristle-bots and hex-bugs. [Balda et al., 2022, Bechinger et al., 2016, Tapia-Ignacio et al., 2021, Porvatov et al., 2021]. Active matter became highly relevant with the Vicseck model in 1995, as this minimalist theoretical model allowed significant progress in predicting the collective motion behavior observed in swarms [Vicsek et al., 1995]. Vicsek's model consists of mathematically describing the position of each member of a collection of active particles with equations that couple the alignment between particles. With this model, phase transitions have been predicted, which is characteristic of many active particle systems, such as bacterial swarms. Since the publication of Vicsek's model, considerable efforts have been made to understand not only active particle systems, but also to study individual active particles through theoretical, experimental, and numerical research. This has contributed to the continued growth and exploration of this dynamic and ongoing field of research.

Figure 1.1: Artistic examples of biological active matter systems: (a) swarm of bacteria, (b) flock of birds, (c) school of fish, and (d) crowd of people. Credit to Midjourney artificial intelligence.

1.1.1 Motile bacteria

Motile bacteria have been widely used to experimentally study both single active particles and systems of interacting active particles. This is largely due to the low cost of growing them and the high reproducibility they provide when experiments are performed in a controlled manner. Two of the most commonly used motile bacteria in the literature on micro-swimmers are *Escherichia coli* (*E. coli*) and *Bacillus subtilis* (*B. subtilis*), both of which have been used in the experiments conducted in this thesis. *E. coli* and *B. subtilis* are non-pathogenic, rod-shaped bacteria that can swim in aqueous media with similar average speeds (approximately 20 µm/s) thanks to the rotation of their flagella that typically measure 10 µm in length. On the one hand, *E. coli* is a gram-negative bacterium that lives naturally in the guts of many mammals, is about 2 µm long and 0.5 µm wide. On the other hand, *B. subtilis* is a 4 µm long and 0.5 µm wide, gram-positive bacterium that lives naturally in soil, water, and also in the digestive tract of some animals. For both bacteria it has been reported that their swimming

strategy is to do a series of runs and tumbles. During a run, they swim in a straight line for a short period of time by the collaborative counterclockwise rotation of their flagella, which organize in a bundle. When one or more of their flagella shortly rotate clockwise, the bundle disassembles and the cell abruptly changes direction [Grognot and Taute, 2021].

Because of the importance of these micro-swimmers in the study of active particle systems, some studies of individual bacterial swimming have been performed. An example is the study by Drescher et al. where the velocity field generated by an *E. coli* bacterium in the liquid medium in which it swims was measured (see Figure 1.2) and it was shown experimentally that the flow generated by this micro-swimmer is well modelled by a pair of forces acting on the fluid, approximately at the body and at the flagellar bundle, approaching the flow due to a force dipole [Drescher et al., 2011]. This study shows that at short distances hydrodynamic interactions with walls or between bacteria become very relevant and must be taken into account when studying particle systems of this type of micro-swimmers.

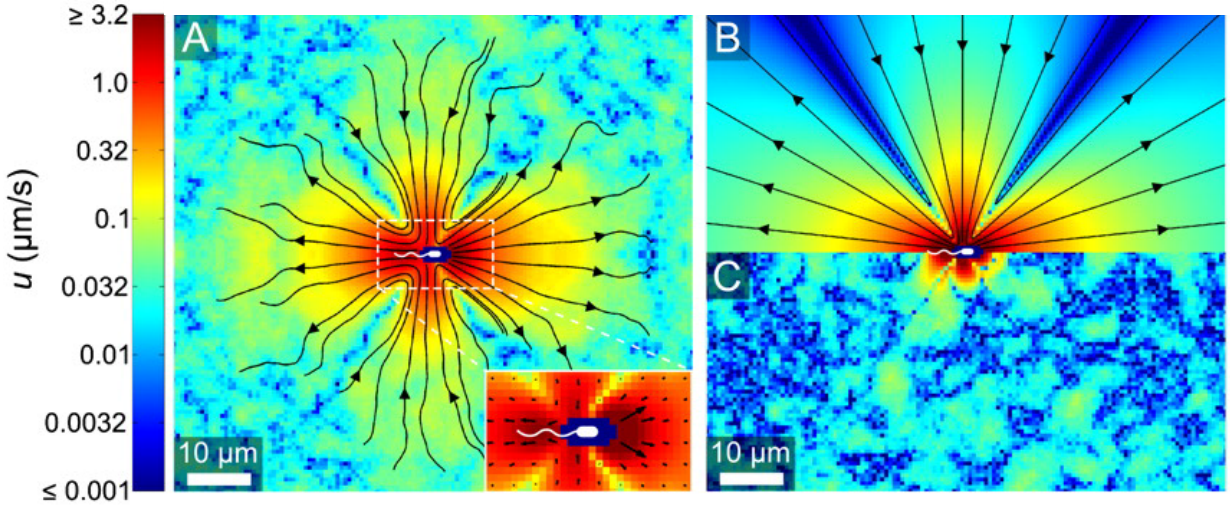

Figure 1.2: Average flow field generated by a single free-swimming bacterium *E. coli*. Black lines indicate the streamlines, and the logarithmic color scheme indicates the magnitudes of the flow velocities. (A) Experimentally measured flow field, the inset shows the anterior-posterior asymmetry of the cell body. (B) Force dipole flow fit. (C) Residual flow field, i.e., the result of subtracting the best-fit dipole model from the measured field. Credit to the work of Drescher et al. [Drescher et al., 2011].

Understanding the flow produced by a single bacterium in an aqueous medium has been fundamental to understand exotic bacteria behaviors. In 2005, the work of DiLuzio et al. reported swimming *E. coli* bacteria moving in a micro-channel of rectangular cross-section (see panel (a) in figure 1.3). In this work, it is observed that these micro-swimmers tend to swim along the right wall of the channel (see panels (b-d) in figure 1.3) and that this effect is stronger when the height of the channel cross section is lower, i.e., when the vertical confinement is greater (see panel (e) in figure 1.3). A year later, the work of Lauga et al. was published, in which they observed that *E. coli* bacteria tend to follow circular trajectories when they are close to a rigid wall (see figure 1.4). In this work, a theoretical model is proposed that can explain and predict not only the phenomenon of circular trajectories, but also the one previously described by DiLuzio et al. The importance of hydrodynamic

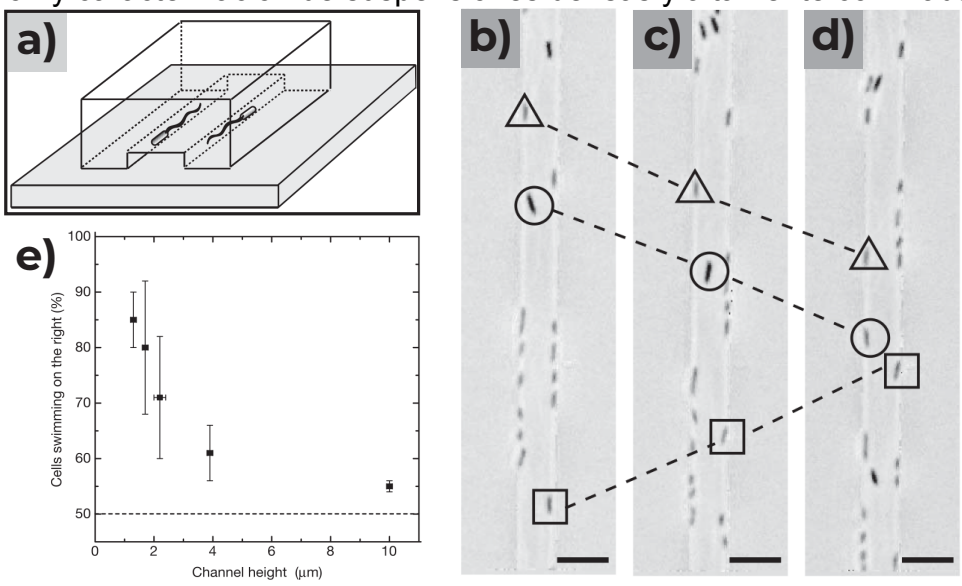

Figure 1.3: (a) Experimental setup of the work of DiLuzio et al. (b-d) Three successive snapshots (0.3 s of time difference) of a micro-channel with *E. coli* bacteria moving along its right hand side. Scale bars correspond to 10 µm (e) Percentage of bacteria swimming on their right side vs. the height of the microchannel cross-section. [DiLuzio et al., 2005]

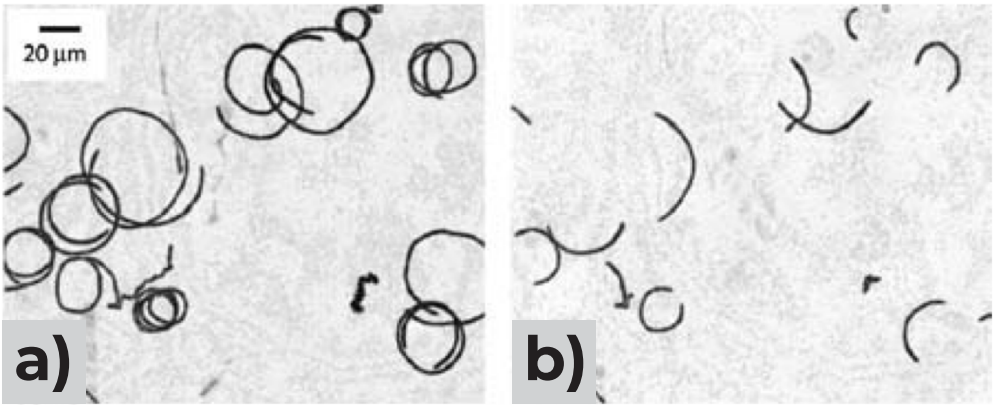

Figure 1.4: *E. coli* trajectories near a solid wall. (a) Trajectory of 8 s and (b) 2 s. Credit to the work of Lauga et al. [Lauga et al., 2006].

interactions in both cases is key, and the tendency of micro-swimmers to approach rigid walls is due to so-called hydrodynamic trapping [Lauga et al., 2006]. The hydrodynamics trapping is originated by the differential rotation of the bacterial body and the flagellar bundle, which causes the appearance of a hydrodynamic torque on the bacteria. By the action of this torque, bacteria near a solid wall tend to swim toward the wall and tracing clockwise circles. Hydrodynamic trapping in micro-swimmers has been reported later even on convex surfaces in the work of Sipos et al. There it was observed that *E. coli* bacteria tend to surround circular pillars when the curvature is low (see figure 1.5) [Sipos et al., 2015]. Hydrodynamic interactions also plays an important role in the interaction between micro-swimmers. Therefore, considerable effort has been devoted to understanding and observing the dynamics of bacterial suspensions. The work of Gachelin et al. studies dilute suspensions

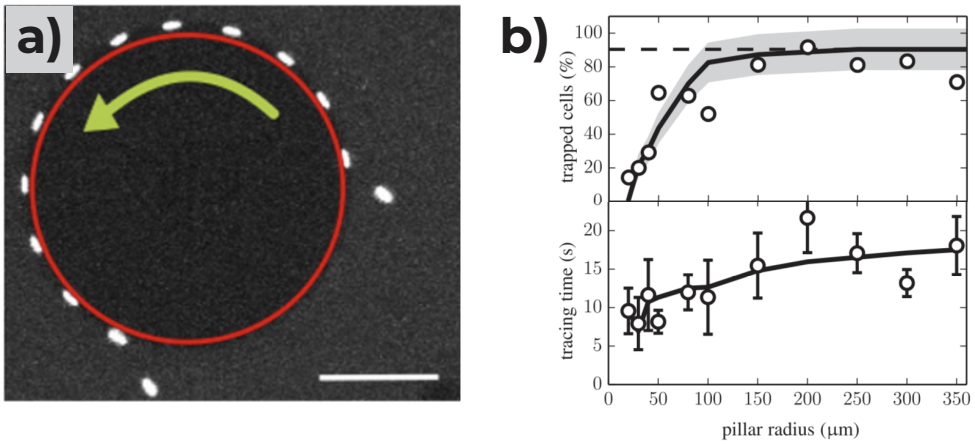

Figure 1.5: a) *E. coli* following the curved surface of a micro-pillar. The elapsed time between each cell position shown is 2.5 s. The arrow indicates the direction of cell swimming. The edge of the abutment is indicated by a solid red line. The scale bar is 100 µm. b) Percentage of trapped cells and tracking time as a function of column radius. [Sipos et al., 2015].

of *E. coli* bacteria. It is shown that as the density increases, a transition from cluster regime to bio-turbulence regime occurs. It was also reported that the bacterial bath exhibits a characteristic length of auto-correlation of velocity that is higher as the concentration increases [Gachelin et al., 2014]. When the concentration of a bacterial bath is high, bio-turbulence type patterns are generated, also referred to in the literature as active turbulence. The work of Wensink et al. focus on the study of the active turbulence generated by a dense suspension of bacteria *B. subtilis* [Wensink et al., 2012], where complex spatio-temporal structures on a scale larger than that of bacteria have been observed (see Fig 1.6). The active turbulence present in the highly fluctuating velocity fields produced by dense bacterial suspensions shares some similarities with inertial turbulence, such as the presence of scaling laws with universal exponents and topological defects, even when individual bacteria are swimming at low Reynolds numbers.

Another more recent approach to the study of active turbulence is that carried out by Henshaw et al. Using the proper orthogonal decomposition (POD) technique, which consists of decomposing a physical field into an orthonormal basis of modes that is optimal for the data set under study, they carried out a modal study of the spatio-temporal structures in velocity and vorticity fields generated by a dense suspension of *B. subtilis* bacteria (see Fig. 1.7). In this study it is shown that the most relevant modes correspond to the structures with longest length scale. Furthermore, it is observed in this study that there are many relevant modes that must be taken into account to fully describe the system, which is similar to the behavior of a flow with inertial turbulence [Henshaw et al., 2023].

1.1.2 Confinement

The hydrodynamic interaction between a dense suspension of micro-swimmers and a rigid wall or a liquid interface creates complex and novel behaviors that have effects on the collective dynamics. Activity patterns have been observed on a scale comparable to the size of

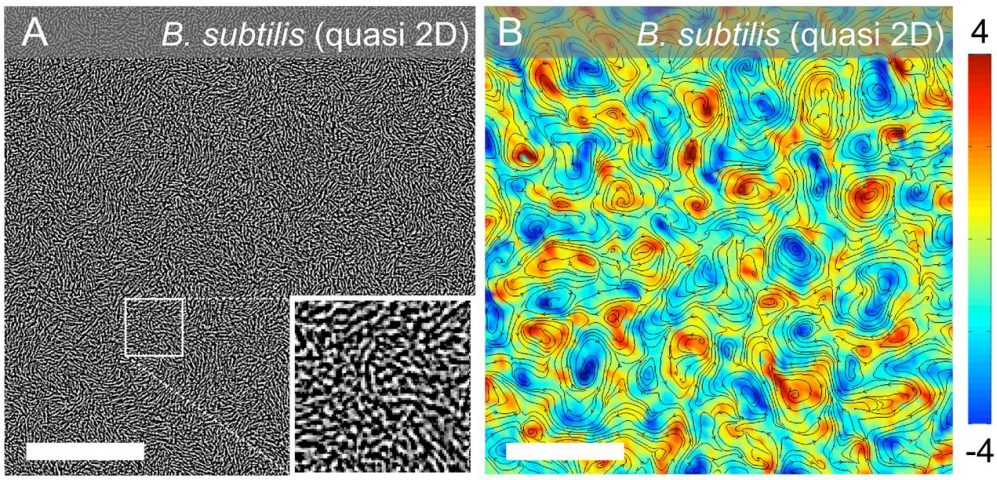

Figure 1.6: (A) Dense suspension of *B. subtilis* bacteria. (B) The color scale shows the normalized vorticity field experimentally generated by the dense suspension of bacteria. Streamlines are shown in black. Figure credit to the work of Wensink et al. (50 µm scale bars). [Wensink et al., 2012]

the confinement, even though it can be much larger than the size of the micro-swimmers. Henshaw's paper also discusses the role of confinement in the turbulent motion generated in a dense suspension of bacteria. In their work, it is mentioned that for the velocity field of the flow produced by the dense suspension, the most relevant POD modes are edge modes, i.e., modes that respect the geometry of the confinement and its characteristic scales (see Fig. 1.8). These modes become significantly more relevant than the turbulence modes with smaller spatial scales observed in the unconfined case. In addition, it has been found that as the confinement decreases, there is a transition from edge modes to turbulence modes [Henshaw et al., 2023].

The importance of confinement is also mentioned the work of Wioland et al. where a high density suspension of *B. subtilis* bacteria is confined in a glass-crushed aqueous droplet surrounded by oil. In this case, the hydrodynamic and steric interactions between the bacteria and the bacteria-interface interaction generate a stable rotating vortex-like collective motion [Wioland et al., 2013]. This study shows that confining surfaces play a crucial role in the dynamics, and patterns generated in self-organizing systems, leading to unexpected behaviors (Fig. 1.9).

1.1.3 Work extraction

Another very important effect observed in active baths of bacteria is rectification. The rectification of Brownian particles has been extensively studied in different areas of physics [Malgaretti et al., 2012, Bartussek et al., 1996]. There are various theoretical and experimental proposals for rectifying Brownian motion performed by micro-swimmers [Fox, 1998]. Concrete examples of this are described in the works of Sokolov et al. [Sokolov et al., 2010] and Di Leonardo et al. [Leonardo et al., 2010], where they managed to rectify the rotation of asymmetric gears immersed in a bath of *B. subtilis* suspension. (Fig. 1.10). In a notable

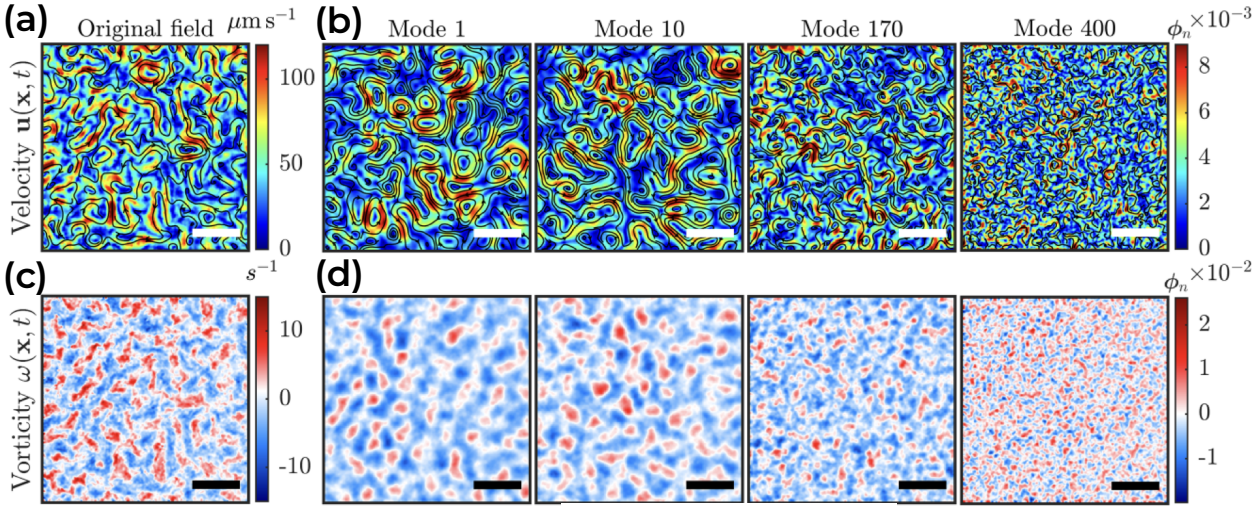

Figure 1.7: (a) Snapshot of the velocity field generated by a dense suspension of *B. subtilis* bacteria. The velocity magnitude is shown in the color scale, and the streamlines are shown in black. (b) POD modes {1, 10, 170, 400} for the velocity field. (c) Snapshot of the vorticity field. (d) POD modes {1, 10, 170, 400} for the vorticity field. The scale bars are 100 µm. Figure credit to the work of Henshaw et al. [Henshaw et al., 2023].

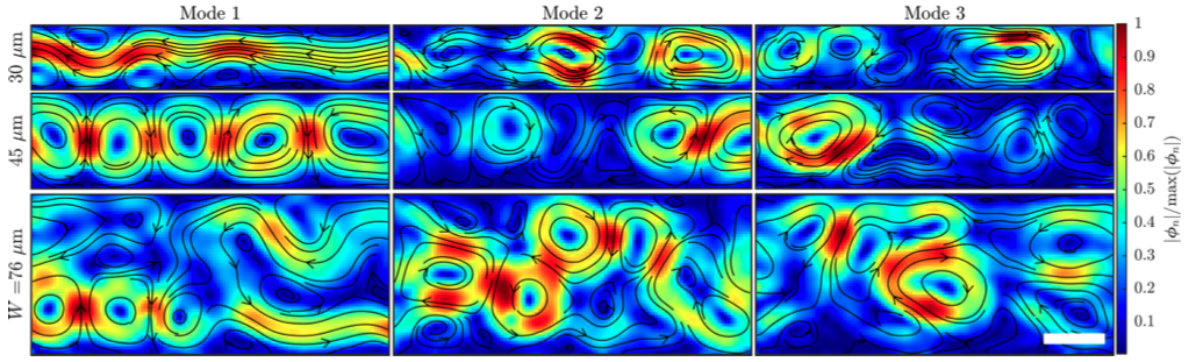

Figure 1.8: First 3 POD modes of a bacterial suspension under 3 different rectangular confinement levels. The width of the channel determines the level of confinement. The color scale shows the magnitude of the velocity normalized to its maximum. The scale bar is 25 µm. Figure credit to the work of Henshaw et al. [Henshaw et al., 2023].

experiment, Sokolov et al. demonstrated that the gear's rotation was attributed to the presence of swimming bacteria in the surrounding environment. When oxygen was removed from the environment, the bacteria lost their motility, and consequently, the gears ceased to rotate (see Fig. 1.11).

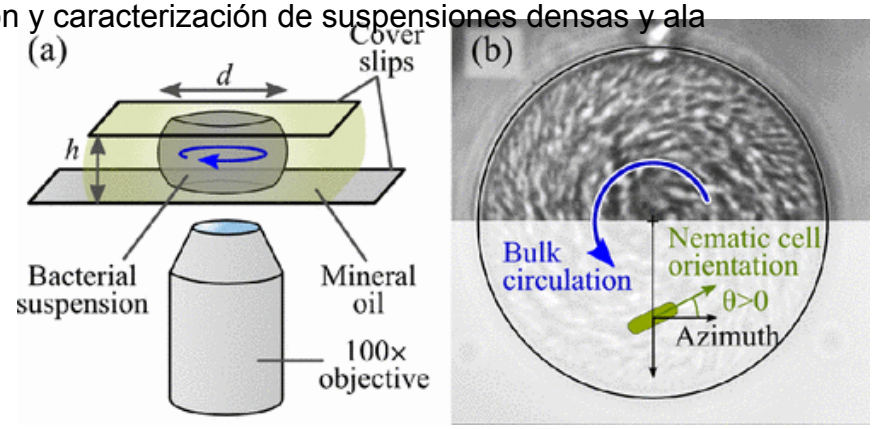

Figure 1.9: (a) Experimental setup with principal confinement dimensions. (b) Snapshot of the experiment. Definition of bacterial orientation relative to the circulating flow. The droplet diameter is 40 µm. [Wioland et al., 2013].

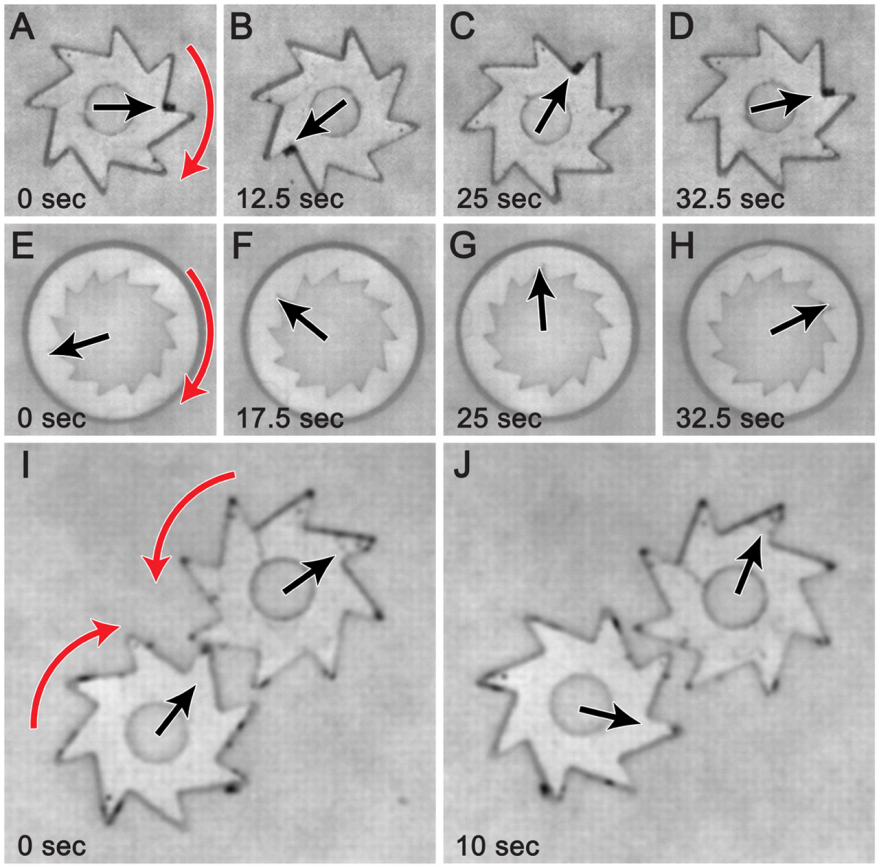

Figure 1.10: Sequences of snapshots illustrating the experiment of Sokolov. (A-D) Rotation of gears with eight external teeth and (E-H) twelve internal teeth. (I) and (J) System of two "meshed" gears rotating in opposite directions. The black arrows indicate the orientation of the gears, and the red arrows indicate the direction of rotation. Gear diameter of 380 µm Figure credit to the work of Sokolov et al. [Sokolov et al., 2010]

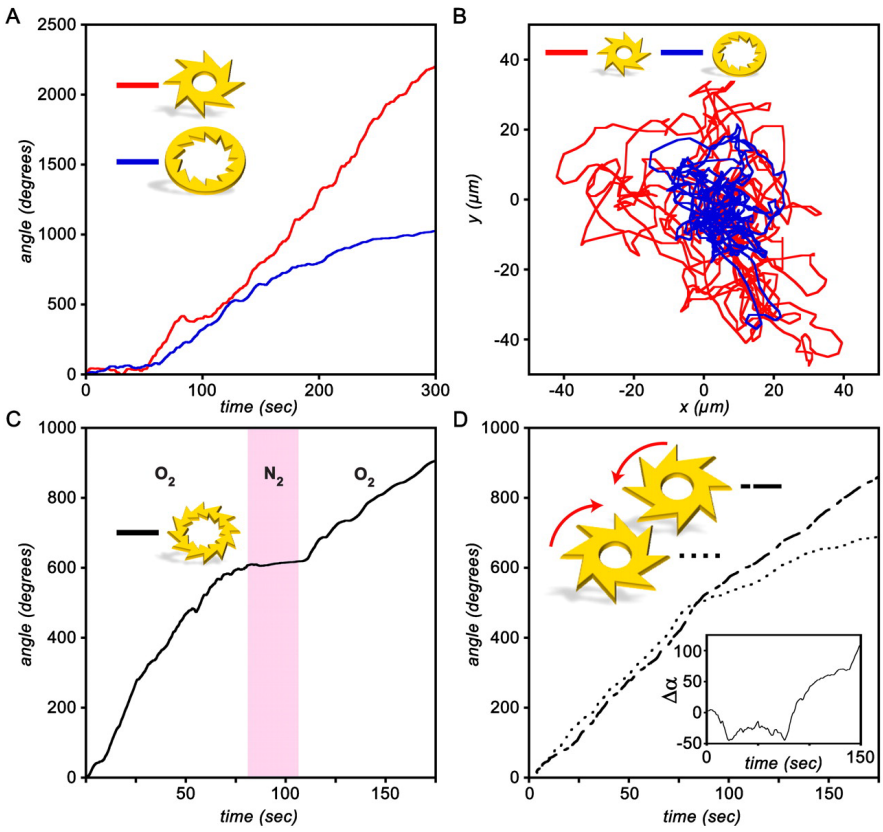

Figure 1.11: Quantification of the gear performance in the experiment of Sokolov et al. (A) Angle of rotation as a function of time (B) Spatial displacement of the center of mass of the gears shown in (A). (C) Angle of rotation as a function of time varying the oxygen concentration in the bacterial suspension. The pink stripe represents the lapse during which oxygen was removed from the system. (D) Synchronous rotation of 2 coupled gears. The inset shows the difference $\Delta\alpha$ in the angles of rotation. Figure credit to the work of Sokolov et al. [Sokolov et al., 2010]

1.1.4 Active carpets

When confinement in one spatial direction is taken to the extreme of completely restricting the movement of micro-swimmers in that direction, we have an active carpet. Active carpets are a dense bath of bacteria confined to move on a flat surface (see figure 1.12). The work of Wu et al. investigates the effect of a quasi-2D bath on passive particles in the bath. The motion of the passive objects was characterized by MSD and it is shown that bacteria play an important role in the motion of these objects [Wu and Libchaber, 2000]. In the work of Kim et al., active motile carpets are studied, where the bacterial body is attached to a plane surface and the flagella are left free and able to promote flow in the surrounding medium. They manage to use this system as a pump that is able to transport fluid from one place to another, and they also make a chemical characterization of the effectiveness of this pump [Kim and Breuer, 2008]. The scheme of an active carpet has been used to theoretically and numerically study the fluctuations of the velocity field produced by bacteria in the surrounding medium when these micro-swimmers remain confined on a surface [Guzmán-Lastra et al., 2021]. The work of

Guzman-Lastra et al. investigated how an active carpet can drive a passive particle that only interacts hydrodynamically with the carpet. The study of active carpets is a promising scheme in which confinement plays a crucial role, and where the hydrodynamic interaction of an active carpet can be studied in a controlled manner and valuable information on bio-turbulence can be obtained, but few attempts have been made to replicate this scheme experimentally.

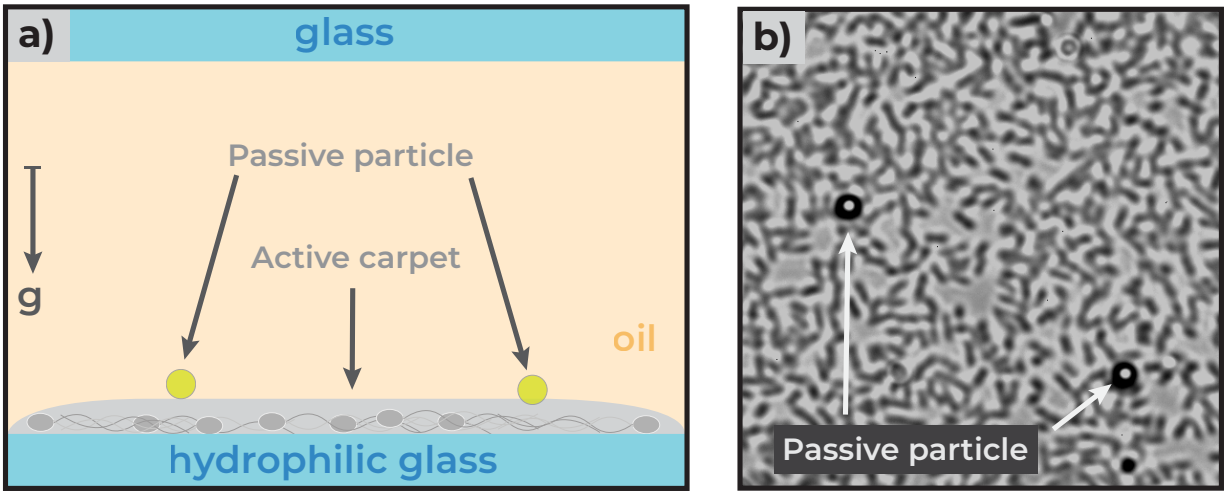

Figure 1.12: a) Schematic of an active carpet. The diagram is not to scale. b) Snapshot of an active carpet.

1.1.5 Active droplets and TBM

In our lab we are able to confine a very dense suspension of bacteria (on the order of 10^{10} bact/mL) in an aqueous droplet immersed in oil, that is what we called an active droplet. If this droplet has a small lubricating layer between its underside and a the substrate, the droplet can self-propel thanks to the flows generated by bacteria, and then we call it a translational bacterial motor (TBM) (see figure 1.13). The bacteria used to generate these motors are *E. coli* or *B. subtilis*, and the oil has been hexadecane, mineral oil, or a combination of both. This emulsion of TBMs is placed in a glass-covered chamber (see Fig. 1.13). Recent experimental results indicate that TBM of *E. coli* in hexadecane, moving on a smooth substrate, exhibit a persitent random motion (see Fig. 1.13), that can be divided into two qualitatively distinct regimes. During the short time-span regime, the motors engage in a ballistic motion, whereby the mean square displacement (MSD) is proportional to time squared (MSD $\sim t^2$). Conversely, during long timescales, the motion is diffusive, where the mean square displacement follows a linear dependence on time (MSD $\sim t$) [Ramos et al., 2020]. Additionally, this report postulates that the motion of the motors is generated by a sliding rolling, which is produced by the activity of the micro-swimmers in the section closest to the substrate. This action generates a shear flow in the thin oil layer between the TBM and the substrate

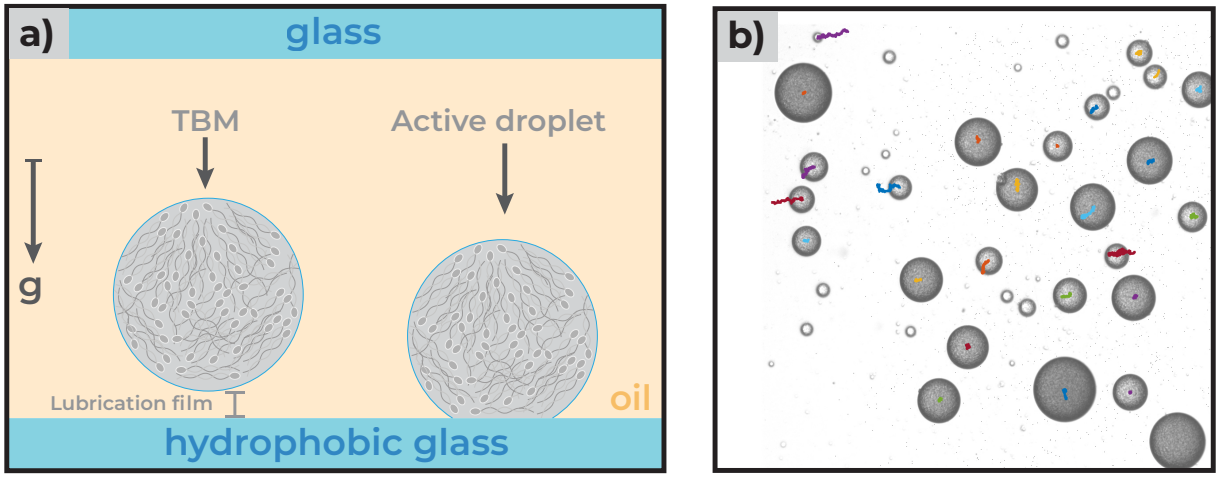

Figure 1.13: a) Schematic of a TBM. Spherical drop with a high density of bacteria inside, immersed in oil. The suspension is covered with glass from above and below. There is a small lubricating layer between the TBM and the bottom glass. The diagram is not to scale. b)Snapshot of the first frame of a 10 minute video with the trajectory of each TBM printed. Random behavior resembling Brownian particles is observed.

1.2 Objectives and structure of this thesis

The main objective of this thesis is to study and characterize dense and highly confined bacterial baths. To this end, we proposed a new way to experimentally generate active carpets and then studied the effect of guiding a passive particle resting on them. We have studied dense suspensions of *E. coli* and *B. subtilis* bacteria trapped in spherical droplets using the POD technique. Finally, we studied the motion of the TBMs by observing their displacement and then attempted to rectify their motion using two types of micro-devices of our own fabrication.

The specific objectives of this thesis are

1. To generate and report a new experimental protocol to generate active carpets.
2. To characterize the MSD of a passive particle driven by an active carpet by fitting the MSD curves to a theoretical model in order to obtain statistical parameters of the active carpet.
3. To characterize flows within an active droplet using the POD technique. From there, to obtain the most relevant modes and verify if there are differences between droplets of *E. coli* or *B. subtilis*.
4. To replicate the movement of the TBMs and observe their MSD. Fit the MSD curves to a theoretical model. To verify the parameter obtained with what is reported in the literature.
5. To fabricate micro-devices using the optical lithography technique to break the spatial symmetry for a TBM.

6. To study the rectification of a TBM when posed in two different micro-devices and see the effectiveness of each device.

Chapter 2

Protocols

To ensure the reproducibility of the experiments performed in this thesis, we have developed reliable protocols. This chapter outlines all the protocols utilized in the experiments carried out in this thesis. These protocols cover the fabrication of microfluidic-devices using optical lithography and the bacterial culture protocol employed. It also describes the data acquisition protocol utilizing our experimental set-up and the analysis of the acquired data.

2.1 Bacterial culture and active droplet/TBM formation

For the experiments detailed in this thesis, we used swimming bacteria, specifically *E. coli* and *B. subtilis*. Prior to the experiment, we cultured each strain from frozen stocks in a nutrient-rich medium until the bacterial population reached saturation. After that, we re-cultivated bacteria from a diluted aliquot of the saturated culture and let the sample grow until it reached its maximum motility, which is typically when the optical density (OD_{600}, a measure of how turbid is the fluid for a light of wavelength 600 nm, which is linearly related to the number density of the bacteria) had a value $OD_{600} \approx 0.5$. Next, the sample is centrifuged to obtain a concentrated pellet of bacteria, which are then re-suspended in a minimal culture medium called *Minimal Medium A* (MMA). This medium allows bacterial swimming but prevents cell division.

To confine a high density of bacteria in a spherical drop, what is done is to take a small drop of the re-suspension and then disperse it in oil. Hexadecane, mineral oil or a combination of the two have been used. The mixture is then shaken vigorously so that the bacterial suspension is transformed into small drops, and then this emulsion is poured into a glass-covered chamber and finally brought to the microscope for observation.

The detailed protocol for each step of this process is outlined below. In addition, the entire process is schematized in figure 2.1.

1. [**Inoculation**] Put 10 µL of a bacterial frozen stock sample in 10 mL of Lysogeny broth

(L.B.) (*E. coli*) or Terrific broth (T.B.) (*B. subtilis*) in a 50 mL Falcon tube.

2. [**Overnight**] Place the sample in an incubator at 30°C and a rotational speed of 200 rpm for 16 hours.

3. [**Re-culture**] Take 10 µL from the previous sample and inoculate a new Falcon tube with 10 mL of L.B. (E. coli) or T.B. (B. subtilis). Put the tube in the incubator until reaching $OD_{600} \approx 0.5$ (between 4 to 6 hours).

4. [**Centrifugation**] After reaching an OD_{600} of 0.5, centrifugate the Re-culture at 4900 rpm for 10 min.

5. [**Re-suspension**] Remove the supernatant and then re-suspend the pellet generated at the centrifugate step with a small amount of MMA (10 µL to 30 µL).

6. [**Emulsion**] Take 10 µL of the Re-suspension and place it in an Eppendorf tube containing 1 mL of oil with wt. 2% of surfactant *span80*. The oil can be hexadecane, mineral oil, or a mixture of both.

7. [**Agitation**] Shake the Eppendorf tube vigorously with your hands. This will separate one large drop into many drops of different sizes.

8. [**To chamber**] Chamber glass must be pretreated with a chemical that makes it hydrophobic (e.g. Aquapel). Take enough emulsion to fill one chamber (typically 100 µL to 300 µL). Cover the chamber with a coverslip.

9. [**To microscope**] Finally, bring your sample to the microscope for observation.

2.2 Micro-fabrication using optical lithography technique

We have access to the optical lithography micro-fabrication technique at the microfluidics laboratory, which is located at the Faculty of Physical and Mathematical Sciences at the University of Chile. By employing the optical lithography process, we are able to fabricate micrometer-scale devices with precision. This technique involves exposing a substrate coated with a thin layer of photo-resist to ultraviolet light, resulting in a controlled and precise micro-device. At our laboratory, we create the designs using the AutoCAD software and execute them using the MLA 100 laser writer machine. We have the capability to produce controlled devices using two types of resins; negative and positive photo-resists. The negative photo-resist remains insoluble to the developer and adhered to the substrate in the area exposed to UV light, whereas the positive photo-resist adheres to the substrate in the region where it was not exposed to UV light while becomes soluble to the developer in the areas exposed to UV light (See Figure 2.2). For positive photo-resist, greater UV exposure results in greater depth, while for negative photo-resist, it results in greater height. Below are the detailed protocols for manufacturing using the available photo-resists.

1. [**Clean**] Clean the glass substrate in the plasma cleaner for 8 min.

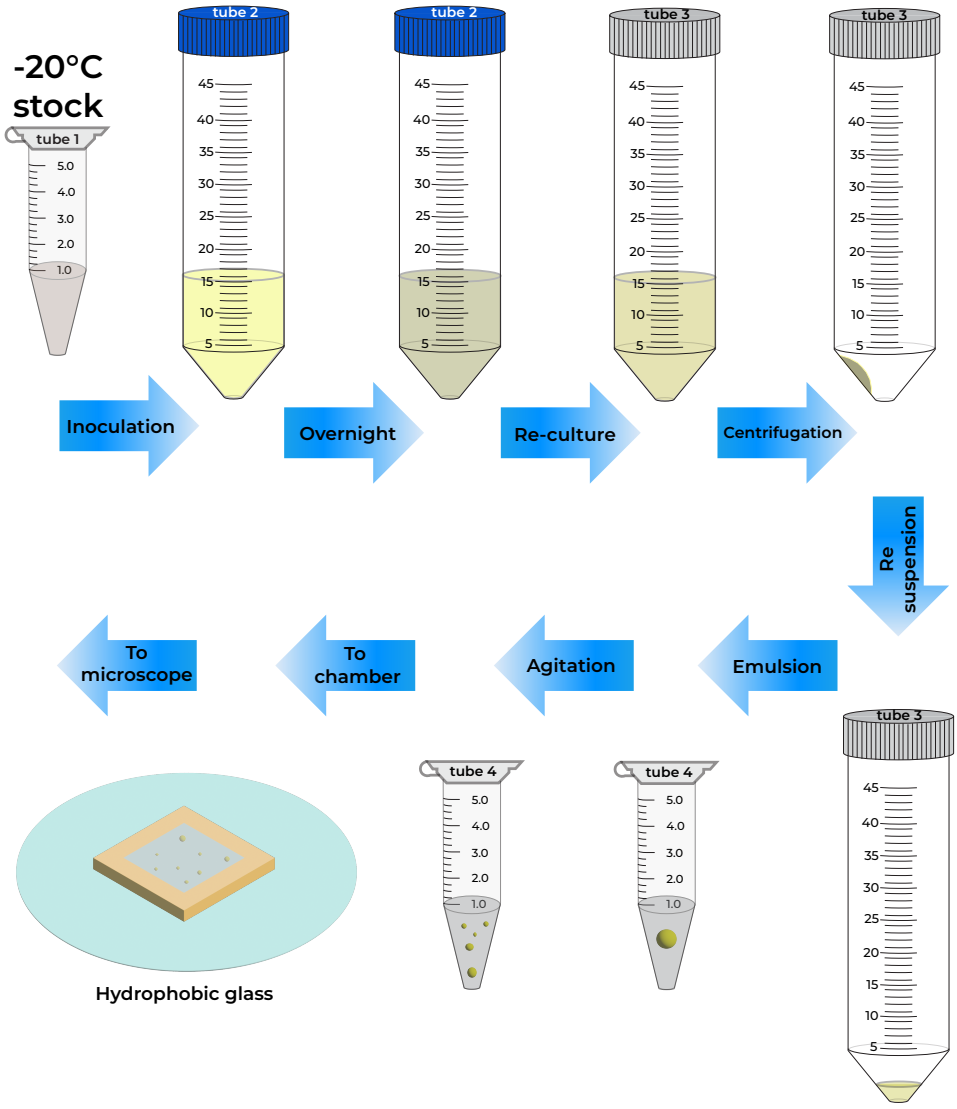

Figure 2.1: Schematic representation of the protocol for bacterial culture plus active droplet and TBM formation. This figure schematically shows the tubes used and the 9 steps indicated in the protocol.

2. [**Cover with photo-resist**] Cover the glass substrate with photo-resist. The amount of photo-resist depends on the glass substrate size and the desired height (see Tab. 2.1).

3. [**Spin coat**] Spin coat the glass substrate covered with photo-resist for 40 s. The spin coat speed depends on the height desired and the specific photo-resist used (see Tab. 2.1).

4. [**Relax time**] Place the sample on a hot plate at 40 °C for the specific duration (see table 2.1).

5. [**Pre-bake**] Rise the temperature to the target temperature. The target temperature depends on the specific photo-resist used. In some cases it is recommended to do a ramp in temperature for better results (see Tab. 2.1).

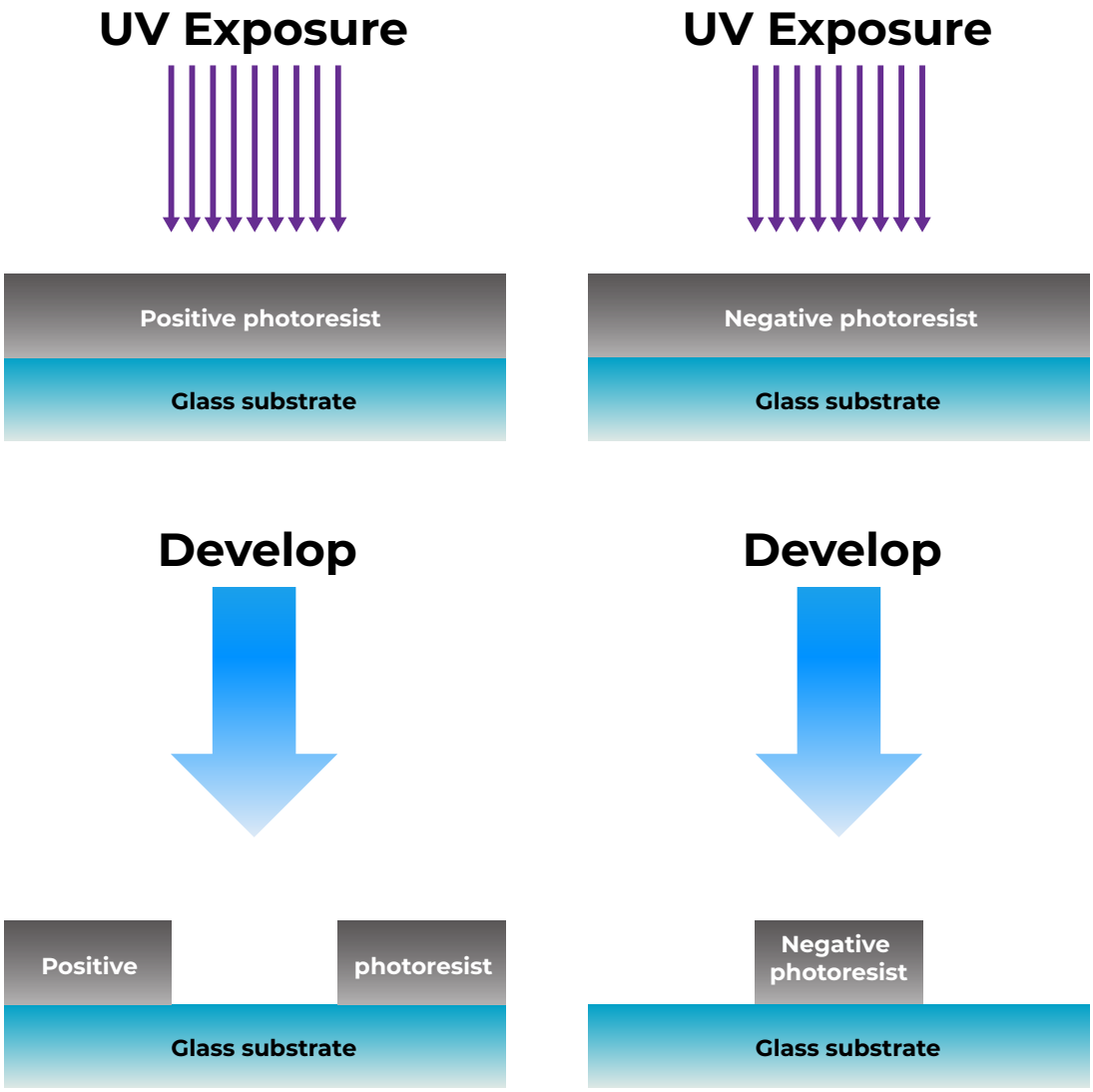

Figure 2.2: Schematic of the difference between positive and negative photo-resist in the context of the optical lithography technique.

6. [**Set exposure parameters**] Put the sample in the optical lithography machine and set the dose and defoc parameters. Dose depends on the desired height and the specific photo-resist used. Defoc depends on calibration (see Tab. 2.1).
7. [**Exposure**] Expose the sample.
8. [**Post-bake**] Place the sample on a hot plate. Rise the temperature to the target temperature. The target temperature depends on the specific photo-resist used. In some cases it is recommended to do a ramp in temperature for better results (see Tab. 2.1).
9. [**Delay time**] Let the sample stand at room temperature for 30 min.

10. [**Develop**] Develop the sample with appropriate developer at the target time. The target time and the developer depends on the specific photo-resist used and the desired height (see Tab. 2.1).

11. [**Hard-bake**] Place the sample on a hot plate and rise the temperature to the target temperature. The target temperature depends on the specific photo-resist using. In some cases is recommended to do a ramp in temperature for better results (see Tab. 2.1).

Step	AZ10XT 15 μm	SU-8 GM1070 15 μm	SU-8 GM1070 50μm	SU-8 GM1070 200 μm	SU-8 GM1075 100 μm	SU-8 GM1075 200 μm
Spin coating	1000 RPM	3000 RPM	1700 RPM	400 RPM	1700 RPM	950 RPM
Relax time	30 min	1 h	1 h	1 h	30 min	30 min
Pre Bake	120 s 110 °C	15 min 65 °C 35 min 95 °C	15 min 65 °C 35 min 95 °C	15 min 65 C 35 min 95 °C	2 min 120 °C	10 min 120 °C
Exposure dose	$1000\frac{\text{mJ}}{\text{cm}^2}$	$475\ \frac{\text{mJ}}{\text{cm}^2}$	$800\ \frac{\text{mJ}}{\text{cm}^2}$	$1300\ \frac{\text{mJ}}{\text{cm}^2}$	$200\frac{\text{mJ}}{\text{cm}^2}$	$500\ \frac{\text{mJ}}{\text{cm}^2}$
Post bake	None	15 min 65 °C 40 min 95 °C	15 min 65 °C 40 min 95 °C	15 min 65 °C 40 min 95 °C	30 min 95 °C	1 h 95 °C
Delay time	None	10 min	10 min	10 min	1 h	1 h
Develop	180 s AZ400K 1:4	2 min PGMEA	4 min PGMEA	22 min PGMEA	3 min PGMEA	7 min PGMEA
Hard-bake	optional	2 h 135 °C	2 h 135 °C	2 h 135 °C	2 h 135 °C	2 h 135 °C

Table 2.1: Parameters in each of the steps of the optical lithography protocol for positive and negative photo-resists at different depths.

2.3 Experimental setup

The experimental setup used in this thesis involves the use of the inverted microscope Nikon TS100F, through which videos are recorded using the professional 4 Megapixel resolution camera Andor Zyla. The captured data is then stored in a computer for further analysis (see Fig. 2.3). This setup allows precise observation and recording of the samples under study, providing high-quality data for subsequent image analysis and interpretation. The TBM samples are suspended in oil and then placed in a custom-made chamber fabricated

using the optical lithography technique with a glass wafer and glass cover-slip, as shown in figure 2.3. The observations are carried out using 10x, 40x, and 60x objectives. The recorded videos are taken at frame rates ranging from 50 fps to 125 fps and stored as a sequence of images for further analysis.

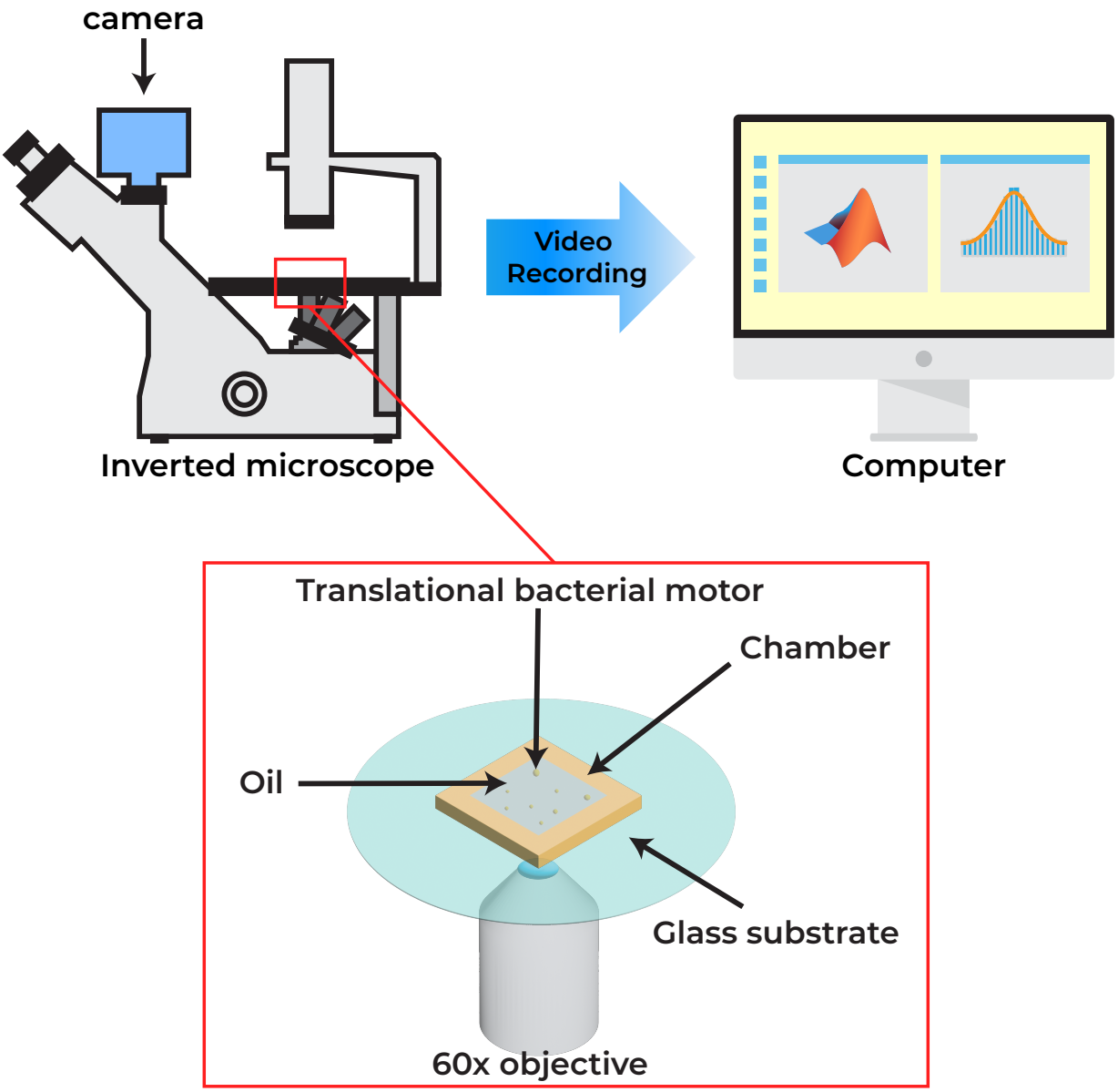

Figure 2.3: Schematic of the experimental setup. Videos are recorded using a camera mounted on an inverted microscope. The camera stores the files in a computer. The inset shows a close-up of the sample to be observed and the lens used in the inverted microscope.

2.4 Image Analysis

The Matlab software was used to track TBMs for each video frame, allowing the determination of their position as a function of time. For image processing, we begin by applying a series of filters such as Gaussian and a flat morphological structuring elements to smooth the edges and improve detection in each image. The detection process uses the Hough transform to identify circles in the image. This approach allows us to obtain the coordinates of the center and the radius of the circle found in each frame. Once the tracking process is complete, we create a mask for each frame to isolate the region of interest, which is the interior of the TBM where bacterial activity takes place. To obtain the velocity field, we employ particle image velocimetry (PIV) by comparing each frame to its succeeding frame (see Fig. 2.4).

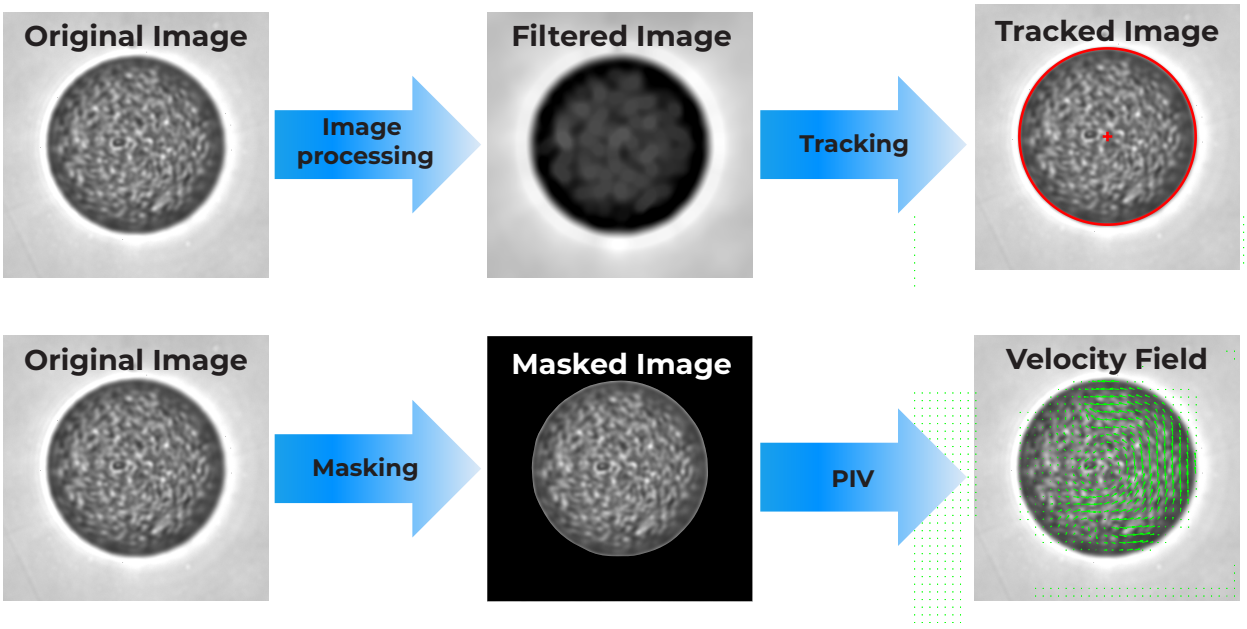

Figure 2.4: Schematic of the image analysis and data extraction from images.

2.5 Data treatment

Image analysis allows to obtain the position of a TBM and the velocity field inside in each frame of the video. The frames of the video are equidistant in time by a difference of $\Delta t = 1/\text{fps}$, where fps are the frames per second of the video acquisition, typically ranging from 10 to 125 for the videos analyzed in this thesis. Thus, for a video with N frames, we obtain the set of positions $\{\mathbf{r}(n\Delta t)\}_{n=1}^{N}$ from the tracking and the set of velocity fields $\{\mathbf{u}(\mathbf{x}, n\Delta t)\}_{n=1}^{N-1}$ The following section details the data treatment procedure and the theoretical models used to predict and understand their behavior.

2.5.1 MSD from tracking

From the set of position it is possible to calculate the mean square displacement (MSD) by means of the following equation

$$\mathrm{MSD}(n\Delta t) = \frac{1}{N-n}\sum_{i=1}^{N-n} \|\mathbf{r}((i+n)\Delta t)) - \mathbf{r}(i\Delta t)\|. \tag{2.1}$$

By defining $t = n\Delta t$, the experimental MSD(t) is defined and then fitted to a theoretical model predicting its behavior. It is important to note from Eq. (2.1) that if $n \ll N$, then the statistical quality of the MSD($n\Delta t$) result is higher, which is equivalent to saying that the experimental MSD(t) is reliable only for $t \ll N\Delta t$.

2.5.2 Theoretical model for the MSD

According to the work of Martens et al., a theoretical model that predicts the MSD of an active Brownian particle reads

$$\mathrm{MSD}(t) = 4D\tau\left[\frac{t}{\tau} - 1 + \exp\left(-\frac{t}{\tau}\right)\right], \tag{2.2}$$

where the parameters of the model are the diffusion coefficient at long times D, and the characteristic time scale of the ballistic motion τ [Martens et al., 2012]. It is important to note that this theoretical model presents 2 regimes. The ballistic regime occurs when $t \ll \tau$, where $\mathrm{MSD}(t) \sim \frac{2D}{\tau}t^2$. From the latter, the short time persistence velocity can then be defined as $v^2 = \frac{2D}{\tau}$. The diffusive regime occurs when $t \gg \tau$, where the model asymptotically approaches $\mathrm{MSD}(t) \sim 4D(t-\tau)$. In some cases, it is useful to express the theoretical model in terms of the parameter v, in which case Eq. (2.2) becomes

$$\mathrm{MSD}(t) = 2v^2\tau^2\left[\frac{t}{\tau} - 1 + \exp\left(-\frac{t}{\tau}\right)\right]. \tag{2.3}$$

It is important to note that the trio of v, D, τ parameters are not independent of each other, and it is possible to go from one pair to another one.

2.5.3 POD from PIV

The proper orthogonal decomposition (POD) technique is the decomposition of a physical field, such as temperature, pressure, or velocity, into an orthogonal basis that is optimal for the measured data set. In this thesis we separate a velocity field $\mathbf{u}(\mathbf{x}, t)$ into N orthonormal modes that satisfy

$$\mathbf{u}(\mathbf{x}, t) = \sum_{n=1}^{N} a_n(t)\mathbf{u}_n(\mathbf{x}), \tag{2.4}$$

where $a_n(t)$ is the temporal amplitude of the $n-$th spatial mode $\mathbf{u}_n(\mathbf{x})$. By defining the inner product

$$\langle \mathbf{u}_n(\mathbf{x}), \mathbf{u}_m(\mathbf{x}) \rangle = \int \mathbf{u}_n^*(\mathbf{x}) \mathbf{u}_m(\mathbf{x}) d\mathbf{x}, \tag{2.5}$$

the modes of the POD technique satisfy the relation $\langle \mathbf{u}_n(\mathbf{x}), \mathbf{u}_m(\mathbf{x}) \rangle = \delta_{nm}$. In the case of the collected data, the position $\mathbf{x}$ and time t is discretized. So when we have a video of N frames and M positions where the velocity field is defined, we obtain the set $\{\mathbf{u}(\mathbf{x}_i, t_n), i \in [1, ..., M], n \in [1, ..., N]\}$. Considering that the velocity field has 2 components, i.e., $\mathbf{u}(\mathbf{x}, t) = (u(\mathbf{x}, t), v(\mathbf{x}, t))^T$, the following data matrix can be generated

$$M = \begin{bmatrix} u(x_1, t_1) & \dots & u(x_1, t_N) \\ \vdots & \ddots & \vdots \\ u(x_M, t_1) & \dots & u(x_M, t_N) \\ v(x_1, t_1) & \dots & v(x_1, t_N) \\ \vdots & \ddots & \vdots \\ v(x_M, t_1) & \dots & v(x_M, \end{bmatrix}. \tag{2.6}$$

Finally, by applying the singular value decomposition (SVD) technique, the matrix is decomposed as $M = A\Sigma U^T$, where the columns of A represent the temporal amplitudes $a_n(t)$ and the columns of U^T contain information about the spatial modes $\mathbf{u}_n(\mathbf{x}_i)$. Σ is a matrix containing in its pseudo-diagonal the singular values σ_n of the decomposition. In the case of applying this technique to a velocity field, the singular values σ_n of the decomposition represent the kinetic energy of the mode $\mathbf{u}_n(\mathbf{x}_i)$ [men, 2023].

Chapter 3

Results

In this thesis, the behavior of a highly confined high-density suspension of swimming bacteria has been studied by means of 3 configurations: active carpets, active droplets and TBMs. Consequently, the first section deals with active carpets, while the second section deals with active droplets and the third one with TBMs. In all cases, the high density of micro-swimmers and the high degree of confinement play a fundamental role in the behavior of these systems.

3.1 Active carpets

Active carpets consist of a high-density suspension of motile bacteria on a flattened volume whose thickness does not allow the bacteria to pass over each other, i.e. the confinement makes them move on a quasi-2D surface. In this configuration, active turbulence-type flows are generated by interactions between the swimming bacteria. Active carpets can drive passive particles positioned above it, which can be used to extract information from the turbulent flow generated by bacteria when trapped in such a configuration.

3.1.1 Formation of active carpets

One result of this thesis is the experimental formation of active carpets. The way in which active carpets are formed is a modification of the point 8 of the active droplets formation protocol (see section 2.1). The glass of the chamber containing the emulsion must be treated to make it hydrophilic rather than hydrophobic. One way to achieve this is to clean the surface of the glass by exposing it to a plasma for 8 minutes. In this way, a droplet configuration of the suspension will be unstable and the droplet content will minimize its interfacial energy upon contact with the glass by wetting the glass in the schematic manner shown in figure 3.1. If the droplet is small enough, a thin film with a high concentration of bacteria is created next to the glass, thin enough to produce a monolayer of bacteria. Figure 3.2 shows 3 successive snapshots as the system move from the droplet configuration to an active carpet. It can be seen how the droplet bursts to go from one configuration to another. The time it takes for the droplets to make contact with the bottom glass of the chamber is approximately 1 min,

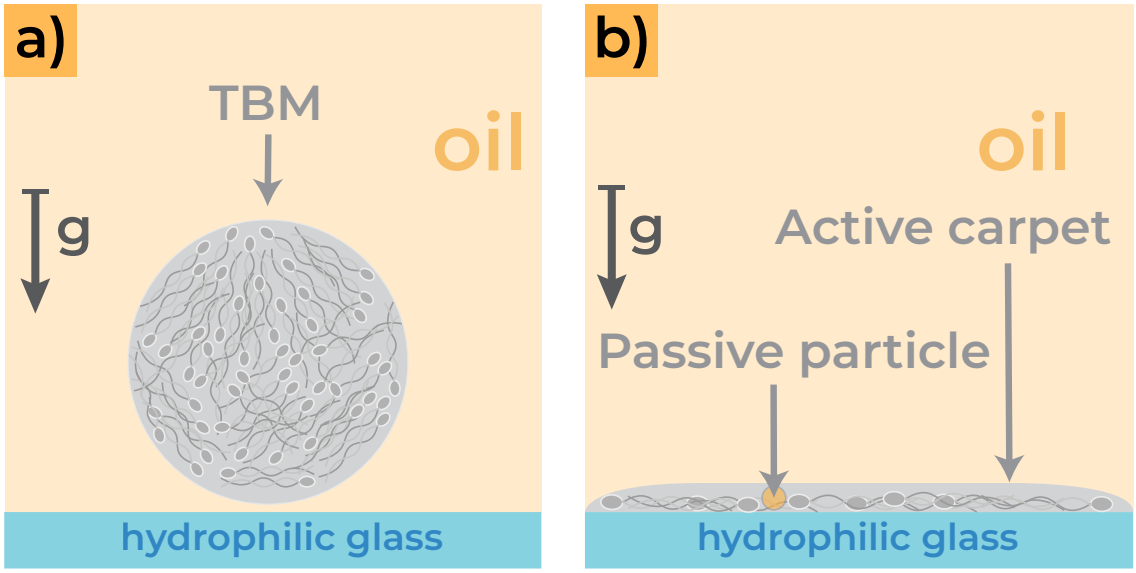

Figure 3.1: Schematic of active carpet formation a) active droplet on a hydrophilic surface. b) Active carpet generated from the active droplet in a).

from there it takes a small fraction of a second (of the order of 60 ms) for the droplets to wet the glass (see figure 3.2), and then the flow inside the active carpet stabilizes 30 s after its formation.

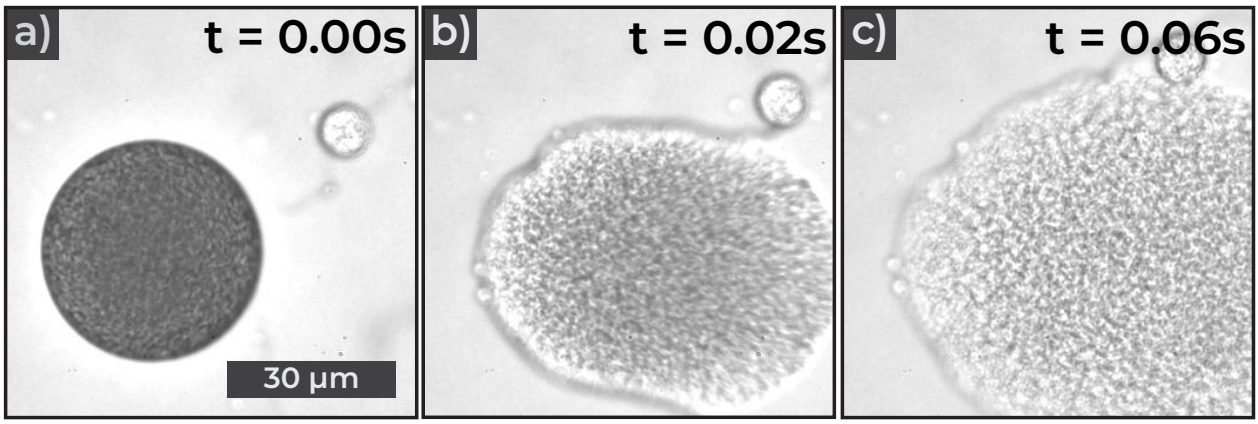

Figure 3.2: Snapshots of the experimental formation of active carpets. a) active droplet on hydrophilic glass surface. b) Snapshot of the active droplet burst. c) Active carpet is formed from the active droplet shown in a).

3.1.2 Passive particle driven by an active carpet

We have observed that when dense suspensions of bacteria are confined in the emulsion droplets, they expel some product that forms spherical shapes of radius r between 0.5 µm and 2.5 µm, and that are not soluble with water nor with oil. Although it is not clear what they are, or even if they are solid or liquid, these spheres can conveniently be used as passive

tracers to obtain statistics of the flows generated by the active carpet. Passive particles of different sizes were detected in each video. A typical trajectory of one of these particles is shown in panel (a) of figure 3.3. The MSD of this trajectory is shown in panel (b) of figure 3.3. It is observed that at short times the MSD behavior is ballistic in time, i.e. the MSD is proportional to t^2, while at long times it is diffusive, and thus the MSD is proportional to t^1. It is also noted that the model proposed in Eq. (2.3) fits the experimental data satisfactorily, adjusting to the ballistic regime at short times, and to the diffusive regime at long times. Thus, it is possible to extract the parameters v, τ and D for each trajectory. This is reflected in figure 3.4, where the fitting parameters v, τ, and D are observed as a function of the radius of the detected particle, r.

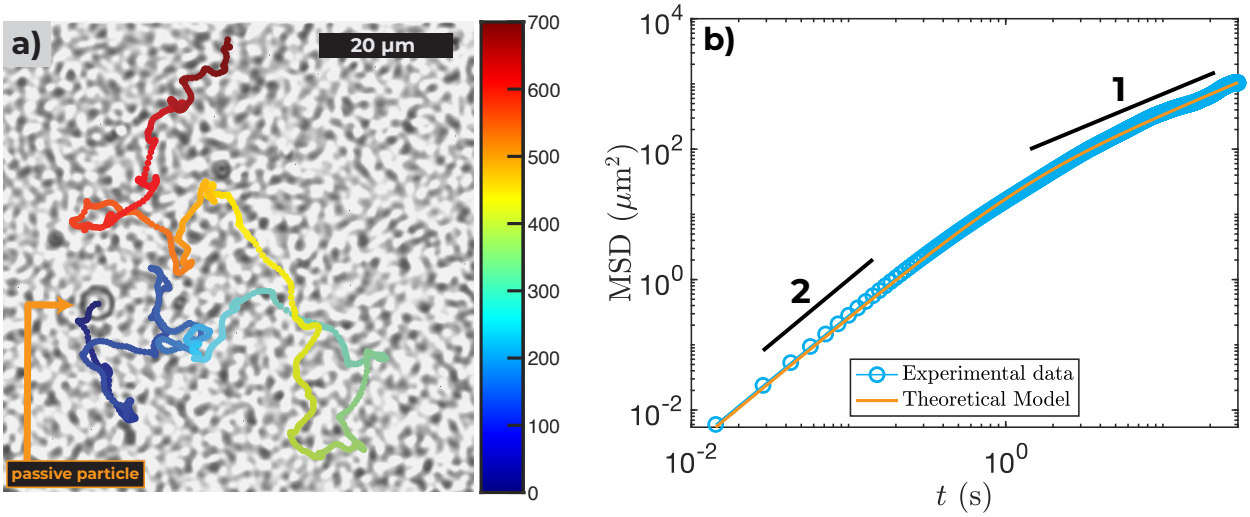

Figure 3.3: a) Trajectory of a passive particle propelled by an active carpet. The time is shown in the color scale in s. b) Experimental MSD of this trajectory with its best fit to the model given by Eq. (2.3) in log scale. Black lines show slope 1 and 2 in log scale for reference.

In panels (a) and (c) of figure 3.4, despite the scatter, a clear growth of the fitted parameters v and D with particle size is observed. However, in panel (b) there is no clear dependence of the τ parameter on particle size. Presumably, the latter is due to the fact that this characteristic time τ is related to the to the persistence time of the active-turbulence flows, which does not change with confinement size since it depends on the strain of bacteria used. It is important to note that the long time diffusion coefficient D of the passive particles driven by the active carpet is mainly due to bacterial activity and not thermal fluctuations. To confirm this, the thermal diffusion coefficient for spherical solid particles at $T = 22\,^{\circ}\mathrm{C}$ and in a fluid medium of viscosity $\eta = 3\,\mathrm{mPa\,s}$ (room temperature and Hexadecane as surrounding media) is shown in orange the panel c) in the figure 3.4. It can be seen that the measured diffusion coefficient is at least 2 orders of magnitude higher, so thermal diffusion can be neglected.

In Patteson's work, the motion of a passive particle driven by an active bath of *E. coli* bacteria is studied. It is found that the diffusivity of the passive particle is due to two effects, one due to the thermal fluctuations of the bath, and the other due to the activity of the bacteria. The first one is measured and agrees with the theoretical prediction, being its contribution much smaller than diffusivity due to bacteria. Furthermore, it is shown that the

diffusivity due to bacteria has a non-trivial dependence on the particle radius r, and that it is even non-monotonic, different from the $1/r$ scaling of the thermal diffusivity. There is an increasing behavior is reported for radii in the range $1-10\,\mu m$, while it is decreasing for radii larger than $10\,\mu m$ [Patteson et al., 2016], which is congruent with the results reported in this thesis. This last result is congruent with one found in this thesis, even though the system of this thesis has a much higher concentration of bacteria, and the passive particle is outside the bacterial bath. The system studied in this section has not been studied experimentally nor theoretically in the literature and opens a new simple system in which to study the bio-turbulence and transport phenomena that occur in this type of bacterial bath.

3.2 Active droplets

This section presents the results of the study of active droplets, a configuration in which the bacterial bath is confined in a spherical volume (see section 2.1). POD analysis was performed on *E. coli* and *B. subtilis* non-motile droplets to better understand the turbulent flow produced by bacteria inside it.

In many cases, it is observed that despite the high activity of bacteria inside the drops, the latter remain in the same position during the entire experiment duration. We believe that this happens because the drop pins to the bottom surface, so there is no oil lubrication layer between the droplet and the glass surface (see figure 1.13). With the drops anchored in place, this is a setup that allow us to study active turbulence in a confined system with spherical geometry. Thus, the velocity field $\mathbf{u}(\mathbf{x},t)$ inside the drop is computed using the PIV technique, with that we compute the vorticity $\boldsymbol{\omega}(\mathbf{x},t) = \nabla \times \mathbf{u}(\mathbf{x},t)$, and then the velocity and vorticity fields are decomposed in POD modes (see section 2.5.3).

It is important to note that the flow generated inside the droplet occurs in 3D, however, we are only able to capture what occurs in one plane of the sphere, thus obtaining a 2D velocity field $\mathbf{u}(\mathbf{x},t)$, which corresponds to a projection of the total velocity field $\mathbf{U}(\mathbf{x},t)$, so $\mathbf{u}(\mathbf{x},t) = \mathbf{U}(\mathbf{x},t)\cdot\hat{\mathbf{i}} + \mathbf{U}(\mathbf{x},t)\cdot\hat{\mathbf{j}}$, where $\{\hat{\mathbf{i}},\hat{\mathbf{j}}\}$ is an orthonormal basis of the plane on which velocity field is computed. From here it follows that we can only obtain a part of the kinetic energy $\mathbb{E}$, which is associated with the 2D velocity field $\mathbf{u}(\mathbf{x},t)$ through the expression $2\mathbb{E} = \int \|\mathbf{u}(\mathbf{x},t)\|^2 dS$. Similarly, enstrophy ε is defined from entropy $\boldsymbol{\omega}(\mathbf{x},t)$ as $\varepsilon = \int \|\boldsymbol{\omega}(\mathbf{x},t)\|^2 dS$.

Drops filled with *E. coli* and *B. subtilis* were analyzed. In the case of *B. subtilis* drops, it was found that they tend to form clusters around the central region of the drops, whereas *E. coli* drops produce a homogeneous suspension without clusters. Figure 3.5 shows an overview of the POD modes decomposition for the velocity and vorticity fields of an *E. coli* drop, while figure 3.6 shows the same for a *B. subtilis* drop. The *E. coli* droplets were analyzed using a 9000 frame video recorded at 70 fps, while the *B. subtilis* droplets were analyzed using a 6000 frame video recorded at 70 fps. Both drops have similar sizes, $67\,\mu m$ for the *E. coli* drop and $62\,\mu m$ for the *B.subtilis* one.

Panels (a) and (b) of figures 3.5 and 3.6 show the kinetic energy and the enstrophy respectively as a function of the n-th mode. It is important to note that this kinetic energy

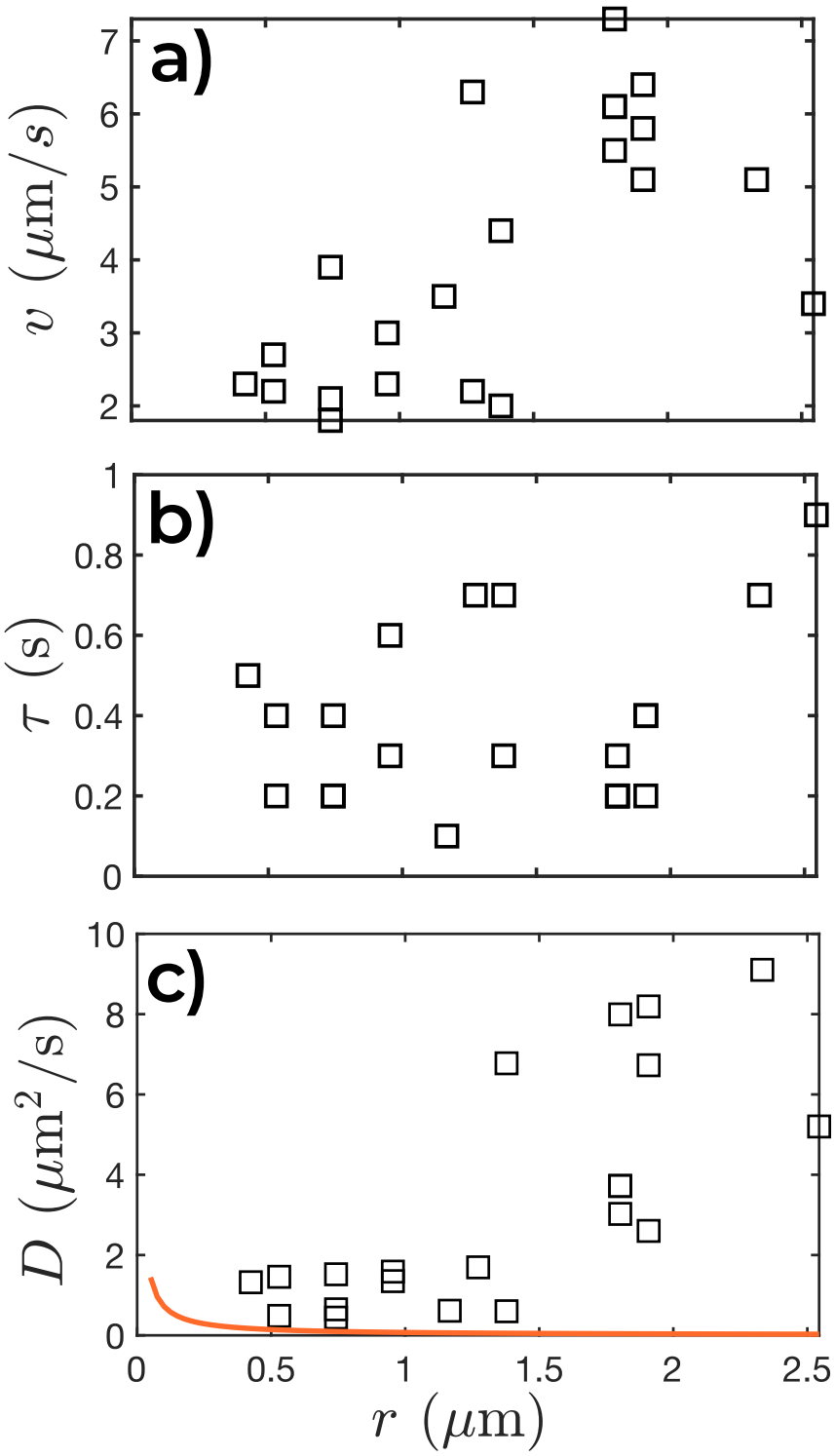

Figure 3.4: Result of the fitting parameters of the model given by Eq (2.3) as a function of its size. a) Persistence velocity v as a function of particle radius r. b) Persistence time τ as a function of r. c) Diffusion coefficient D as a function of r. The orange line shows the thermal diffusion coefficient $D_{th} = \frac{k_B T}{6\pi\eta r}$ at $T = 22\,^{\circ}\mathrm{C}$ and $\eta = 3\,\mathrm{mPa\,s}$.

and enstrophy are obtained from the velocity field $\mathbf{u}(\mathbf{x}, t)$, which is two-dimensional because the images are focused on a cross section in the equatorial zone of the droplet. However, since

the bacteria can move in any direction within the droplet, the velocity field they generate must be three-dimensional, and therefore the calculated kinetic energy and enstrophy from the velocity field $\mathbf{u}(\mathbf{x}, t)$ represent only a portion of the total kinetic energy and enstrophy. The numerical value of the kinetic energy and enstrophy associated with the n-th mode tells us how relevant that mode is relative to the others. We use it as a characterization of the relevance of a particular mode. From that, figures 3.5 and 3.6 shows that the relevance of the modes decay slowly for *E. coli* and *B. subtilis* drops. This indicates that the flow produced by the bacteria inside the active droplets resembles that of active turbulence, which is also typical of inertial turbulence [Henshaw et al., 2023].

The n-th spatial POD mode can be expressed in polar coordinates as $\mathbf{u}_n(\mathbf{x}) = \mathbf{u}_n(r, \theta)$ so that it is possible to calculate a radial mean of the velocity magnitude given by

$$\langle \|\mathbf{u}_n(r)\| \rangle = \frac{1}{2\pi} \int_0^{2\pi} \|\mathbf{u}_n(r, \theta)\| d\theta. \tag{3.1}$$

It is observed in the panel (c) of figure 3.5 and 3.6 that the 8 most dominant POD modes are such that $\langle \|\mathbf{u}(r)\| \rangle$ vary over distances that are of the order of the radius of the droplet. This types of POD modes are called edge modes in the literature [Henshaw et al., 2023]. This confirms recent findings that show that the external confinement, even when it can be one order of magnitude larger than individual bacteria, dominate the topology of the turbulent active flows [Henshaw et al., 2023]. This is not the case for turbulence modes, where the radial velocity shows noise fluctuations around a constant value when looking at its dependence on any spatial direction.

The velocity magnitude of the POD decomposition, $\|\mathbf{u}_n(\mathbf{x})\|$, is shown in panels (d), while the vorticity magnitude of the POD decomposition, $\|\boldsymbol{\omega}_n(\mathbf{x})\|$, is shown in panels (e) in the figure 3.5 for an *E. coli* drop and in figure 3.6 for a *B. subtilis* drop. The velocity and vorticity magnitude of the POD modes show that the flow generated by the micro-swimmers is qualitatively different between an *E. coli* drop and a *B. subtilis* drop. It is observed that the edge modes, i.e., the first ones, in the *B subtilis* drop are less symmetrical than in the *E. coli* drop, furthermore, the panel (c) in figures 3.5 and 3.6 shows that the activity peaks of *E. coli* drops for the first eight modes are more homogeneously distributed in space than for the *B. subtillis* drops. In contrast, the activity in the *B. subtilis* drop is concentrated at the edges. Presumably, such edge activity is due to 2 reasons. The first is due to the elongated shape of *B. subtilis* bacteria compared to *E. coli*, which makes them more likely to align with the drop surface. The second reason is the presence of clusters in the central part of *B. subtilis* drops, which tend to move as a rigid body. Finally, it is important to note that the higher the number of frames in a movie, the higher the statistical quality of the POD modes. This is the reason for the difference in smoothness between figure 3.5, which was created from a 9000 frame movie, and figure 3.6, which has 6000 frames.

These results on the decomposition into POD modes of the velocity field generated by a dense bath of bacteria under spherical confinement are new in the field of active turbulence and open new possibilities for study. New measurements are needed to systematize the results obtained and to observe the behavior of the decomposition into POD modes varying the density of the bacteria, the size of the confinement and the strain of the bacteria.

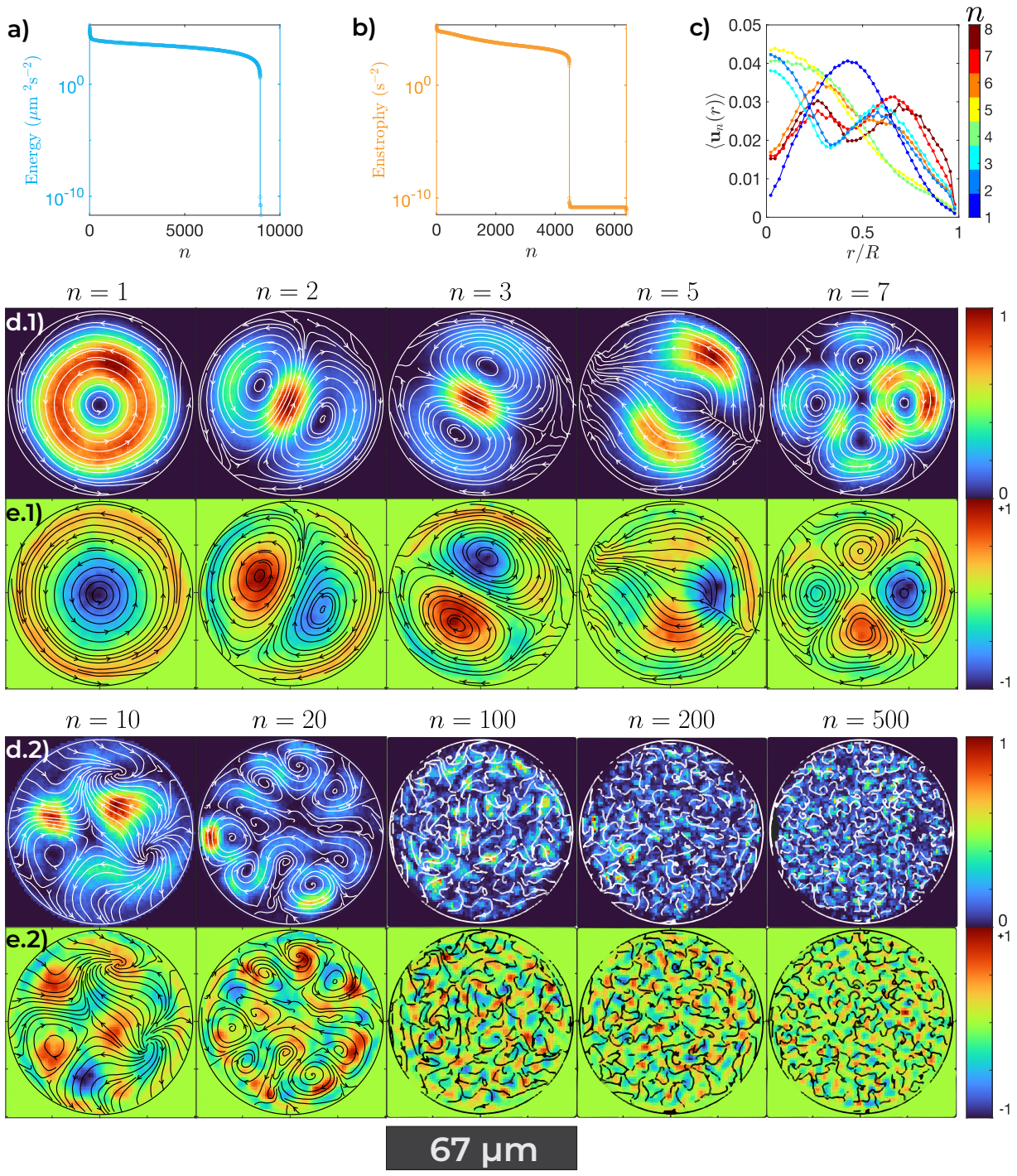

Figure 3.5: Analysis of a 9000 frame video of an active droplet of *E. coli* bacteria using the POD technique. a) Kinetic energy of the velocity field modes b) Enstrophy of the vorticity field modes c) Radial velocity distribution of the first 8 modes. d) POD velocity field modes, normalized velocity magnitude in color scale, white stream-lines. e) POD vorticity field modes. Normalized magnitude of the vorticity field in color scale, black streamlines.

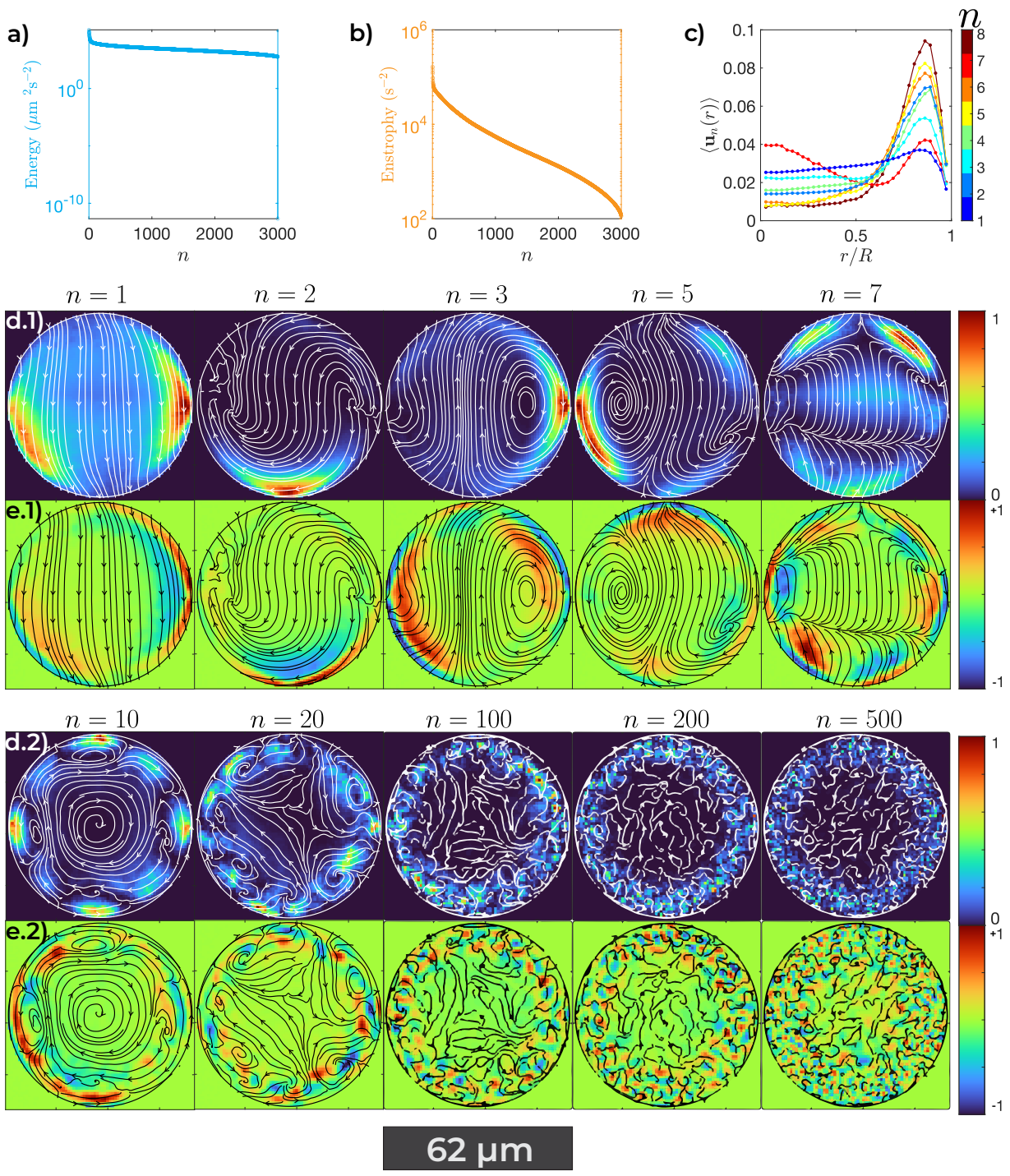

Figure 3.6: Analysis of a 6000 frame video of a TBM of *B. subtilis* bacteria using the POD technique. a) Kinetic energy of the velocity field modes b) Enstrophy of the vorticity field modes c) Radial speed distribution of the first 8 modes. d) POD velocity field modes, normalized velocity magnitude in color scale, white streamlines. e) POD vorticity field modes. Normalized magnitude of the vorticity field in color scale, black stream-lines.

3.3 TBMs

When an oil-immersed TBM is placed on a smooth glass surface, it can be observed that it is capable of self-propulsion due to the turbulent flow created by the bacteria inside. Panel

(a) of figure 3.7 shows the typical trajectory of a TBM, while panel (b) shows the MSD associated with this trajectory along with the best fit of the theoretical model described by Eq. (2.2).

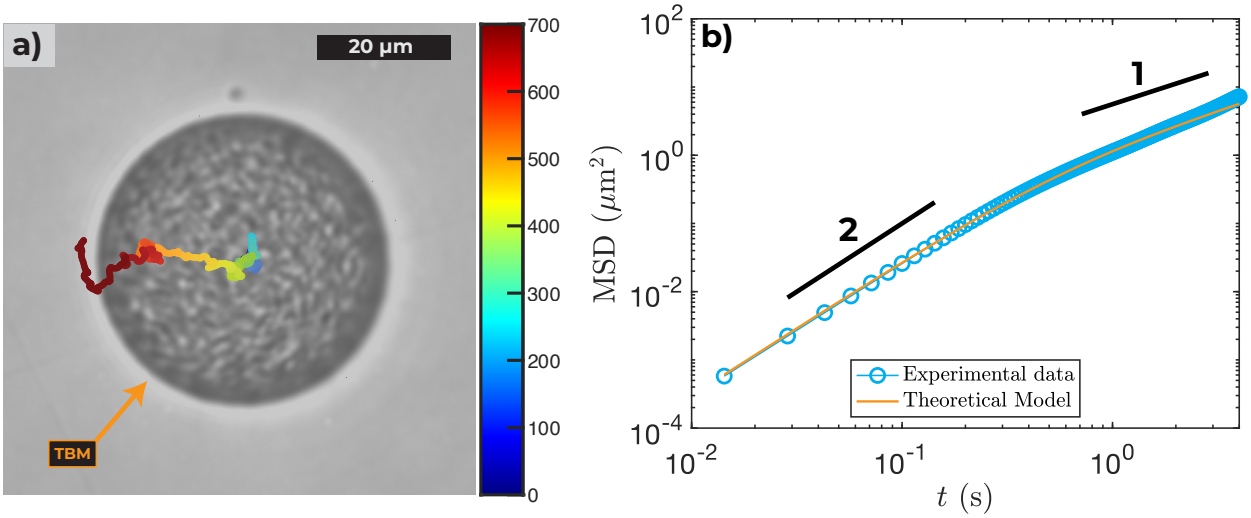

Figure 3.7: a) Trajectory of a TBM. The time is shown in the color scale in s. b) Experimental MSD of this trajectory with its best fit to the model given by Eq. (2.2) in log scale. Black lines show slope 1 and 2 in log scale for reference.

By analyzing TBMs of *E. coli* with similar density (around 8×10^9 bact/mL) but different radius, we fit their MSD curves to the theoretical model of equation (2.2) to each drop and extract their parameters v, D, τ. Figure 3.8 shows these parameters as a function of TBM radius. This figure shows a large scatter of the parameters v, D and τ, which is consistent with what has been reported in the literature [Ramos et al., 2020]. We believe that the dependence of τ on radius is constant, since it depends on the persistence time of the active-turbulence flows, which is presumably inherent to the species, as in the case of active carpets (see section 3.1). We believe that the scatter in the v and D parameters is due to fluctuations that occur due to the biological nature of the system, and that more experimental data are needed to increase the statistical richness.

3.3.1 Fabrication of ratchets

Achieving rectification requires not only temporal irreversibility but also a break in spatial symmetry, both at the same time. Bacterial baths are out of thermodynamic equilibrium systems, so the temporal irreversibility is present. We have explored two approaches to break spatial symmetry: the first involves the use of a ratchet-type substrate, while the second utilizes ratchet-type channels. For the first approach, we developed an original technique tailored to the capabilities of our fabrication methods. As for the second approach, we have also devised a novel technique to implement it.

In order to achieve the required surfaces, the AZ10XT positive photo-resist was chosen because of the high precision obtained for designs that have variations in the 2 micron range. The first step was to create a calibration curve by varying the 2 parameters that the MLA100

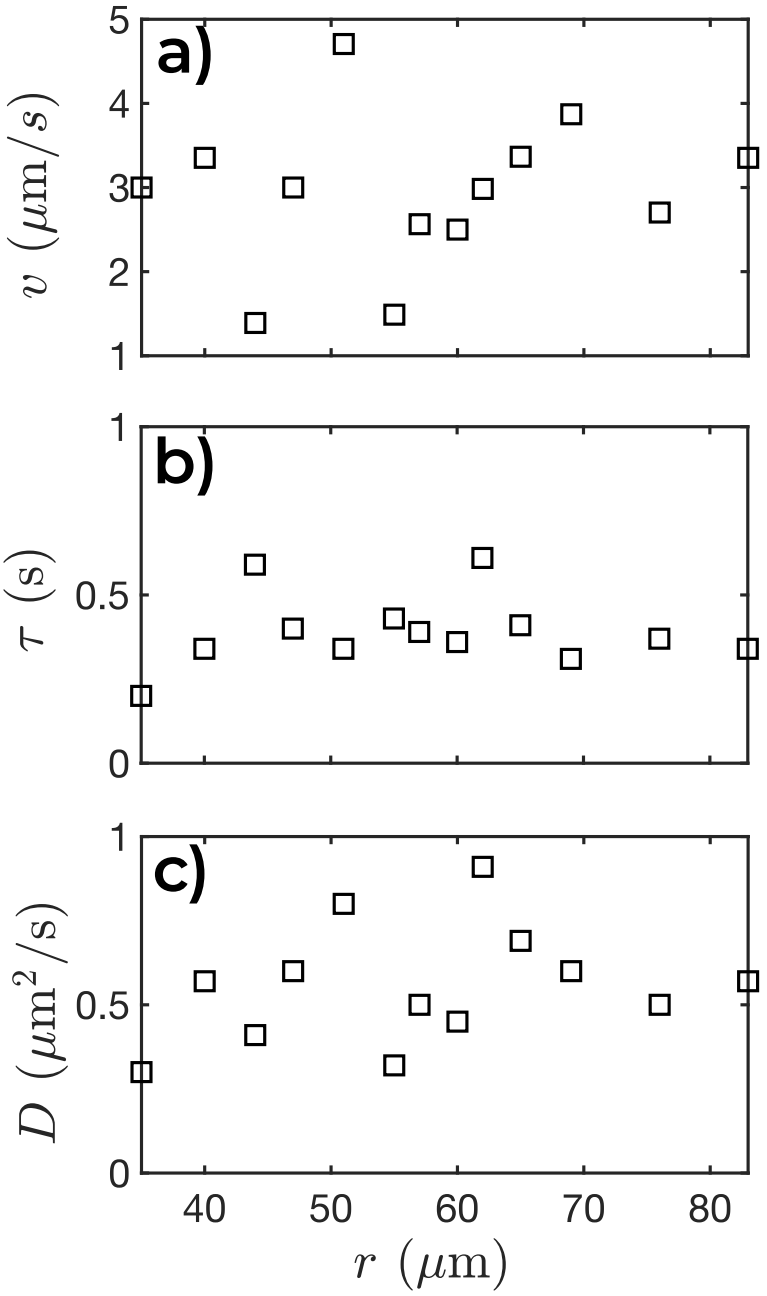

Figure 3.8: Result of the fitting parameters of the model given by Eq (2.2) as a function of its size. a) Persistence velocity v as a function of particle radius r. b) Persistence time τ as a function of r. c) Diffusion coefficient D as a function of r.

machine has; dose and defoc. Dose is measured in units of energy per area and measures the energy that the laser prints on the resin. Defoc is a parameter that measures where the laser is focused.

A glass wafer coated with a 16 µm thick layer of positive photo-resist was used to construct the calibration curve. On it, 2 µm wide stripes were exposed, varying the dose and defoc parameters. After developing the sample according to the protocol (see 2.2), polydimethylsiloxane (PDMS) was used to produce a negative of the printed stripes. The PDMS

was cured and detached from the photo-resist layer, cut and observed from the side under a microscope, to measure the depth h of the printed stripes.

The result is shown in figure 3.9. Panel (a) shows the depth h of the printed stripes as a function of dose. The color of each curve indicates the defoc parameter used in the color bar. Panel (b) shows the average of these curves, since there is no significant difference between curves with different defoc. For the fabrication shown in this thesis, defoc = 0 was chosen.

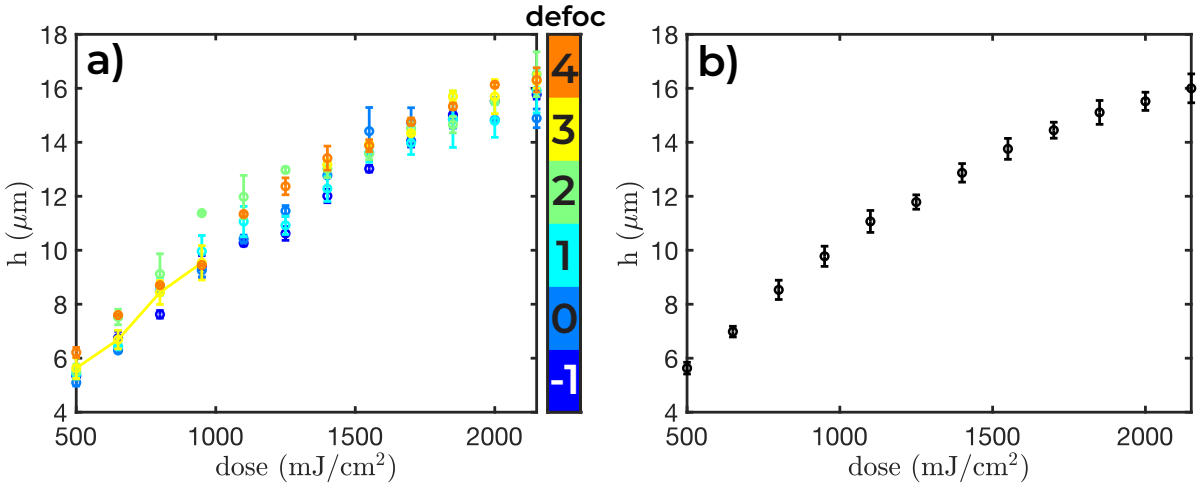

Figure 3.9: Calibration curve for optical lithography on AZ10XT positive photoresist. a) Depth as a function of dose for each defoc parameter. b) Depth as a function of dose by averaging the different defoc curves in (a).

3.3.2 Ratchet-type substrate

One way to break the spatial symmetry in the flow generated by a TBM is to place it on an anisotropic surface. In this sense, the ratchet-type substrate is a type of surface fabricated in the laboratory using the optical lithography technique. This micro-surface consists of the repetition of a staircase to obtain a sawtooth-type surface. To achieve that, a positive photo-resist is used in which a distance $m\delta$ is divided into m spaces of distance δ (ranging from 2 µm to 5 µm) that successively reduce the energy dose by a small amount (typically 100 mJ cm^{-2}). Note that in this type of surface, the asymmetry is in the direction of gravitational acceleration. This process is shown schematically in figure 3.10.

During the development process, the involved chemistry smoothens the staircase, resulting in a smoother surface. This process has allowed to produce ratchet-like surfaces in a very precise manner, controlling only the dose parameter. Some results are shown in figure 3.11, where the schematic design and photos of a real result are shown. The profiles of the ratchet-like surfaces were obtained by using the surfaces to cast a PDMS block, then removing and cutting the PDMS to observe it from the side under a microscope.

Once the ratchet-type surfaces are obtained, the TBMs were placed on them. In this way, spatial symmetry is broken in the system. It is expected that the TBMs will be able to rectify

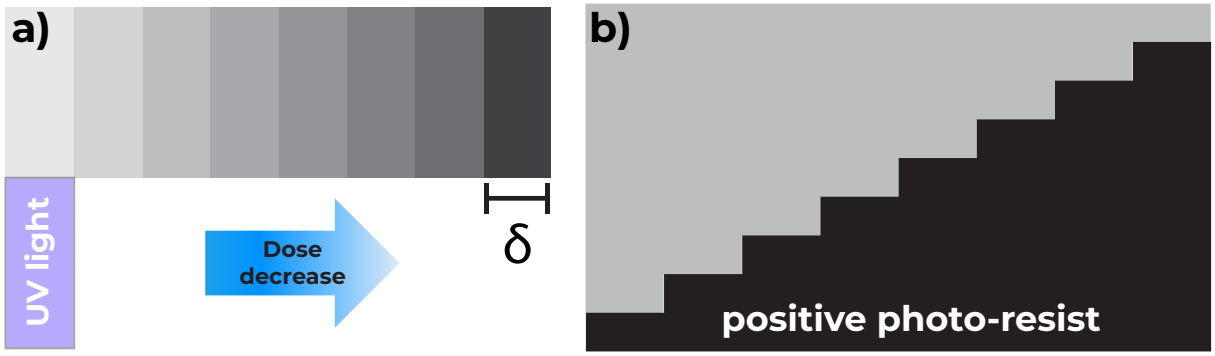

Figure 3.10: Schematic of the ratchet surface fabrication process. (a) Pattern generated in gray scale and optical lithography exposure stripes decreasing dose to the right. Light is more dose, dark is less dose (b) Schematic side view of the expected pattern.

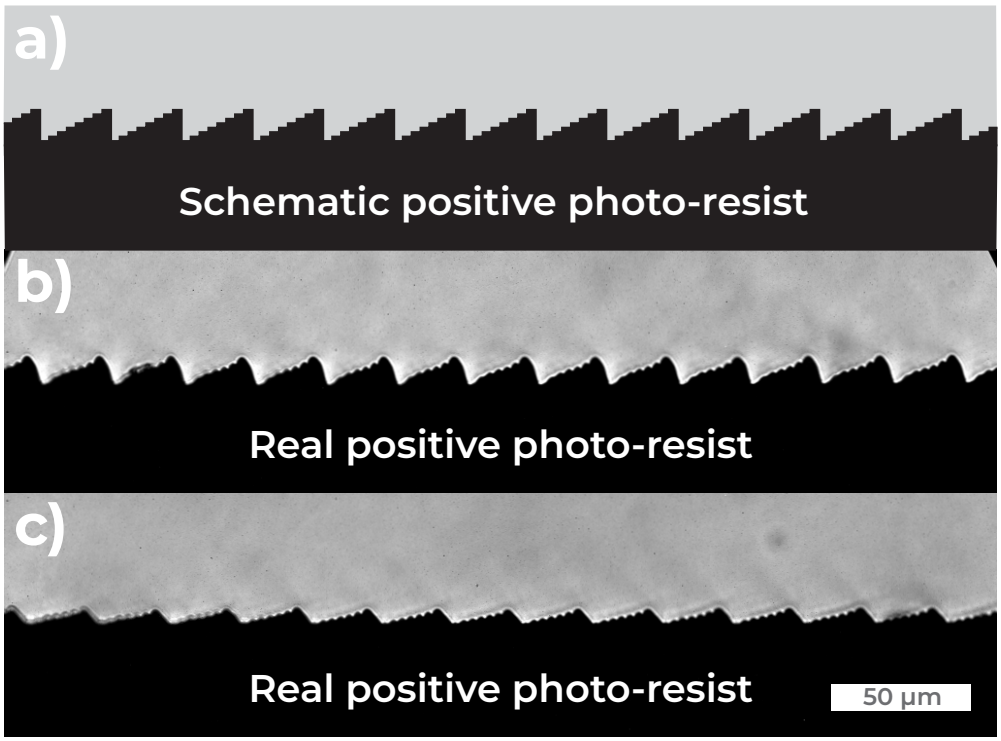

Figure 3.11: a) Design schematics b) and c) results of the micro-fabrication with positive photo-resist using optical lithography with different dose step parameters.

their motion in the direction of the asymmetry of the ratchet surface. If the energy of the TBM is not large enough, it will remain in Brownian motion along the perpendicular direction of the asymmetry. This is exactly what is observed in figure 3.12, where the x-position of the TBMs remains constant, i.e. in the same 'potential well', but different displacement phenomenologies occur along the y-axis. For this experiment, we suspended several TBMs wich have radius r between 12 µm and 24 µm with the same density (around $n \sim 9.8 \times 10^8$ bact/mL) on the ratchet-type substrate whose maximum height is 8 µm and the width of the 'potential well', i.e., the periodicity width is 20 µm, such as that shown in panel c) of figure

3.11.

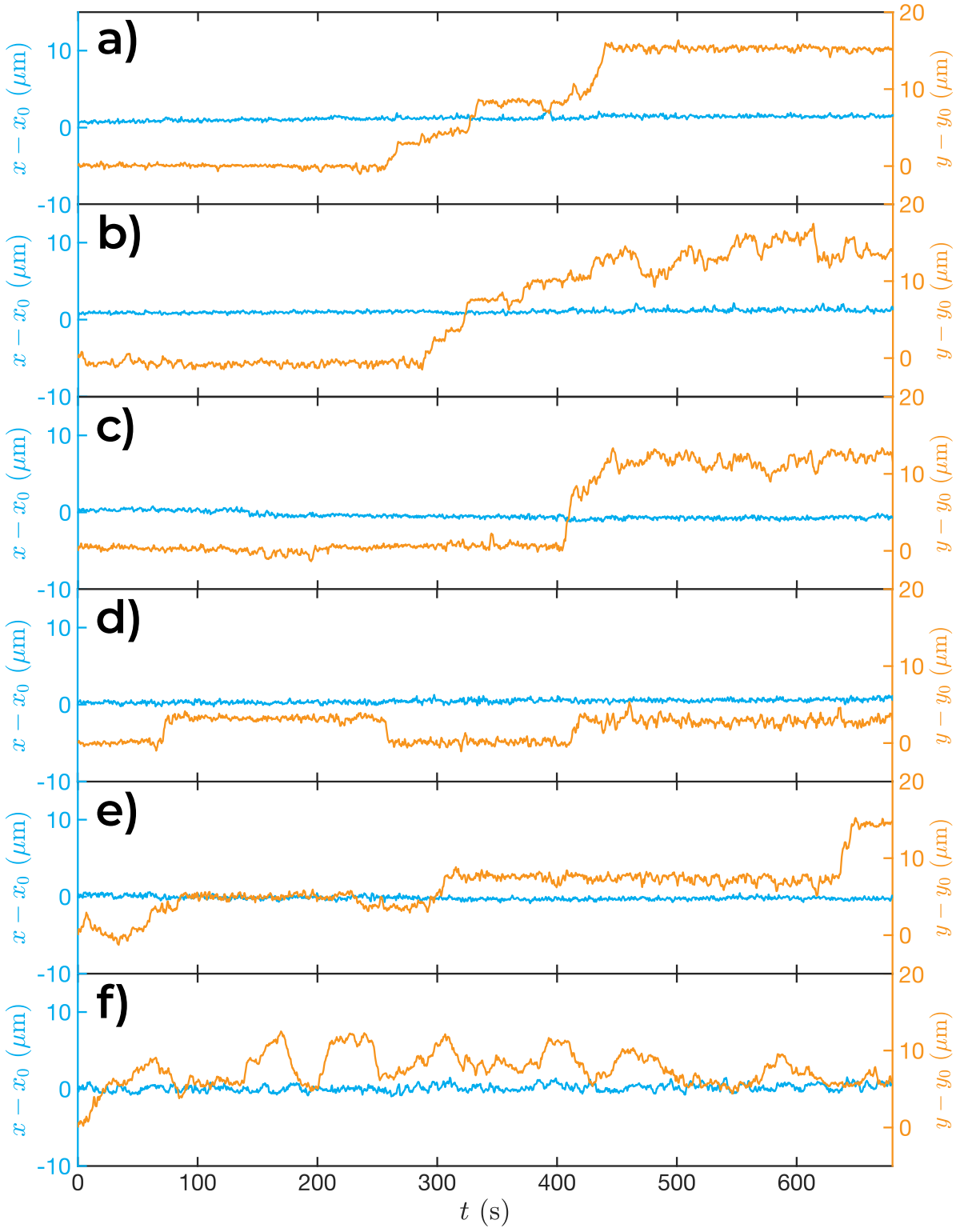

Figure 3.12: 6 different trajectories of a TBM resting on a ratchet-like surface, where the displacement is on the y-axis. The radius r of each TBM are given by a) $r = 12\,\mu\text{m}$, b) and c) $r = 14\,\mu\text{m}$, d) $r = 15\,\mu\text{m}$, e) $r = 21\,\mu\text{m}$ f) $r = 24\,\mu\text{m}$. The density in all cases is given by $n \sim 9.8 \times 10^8 \text{bact/mL}$.

Panels (a-c) of figure 3.12 show 3 cases of similar behavior in TBMs on ratchet-type surfaces. It is observed that from a certain moment on, all these motors move along the y-axis. The change of state is moderately abrupt. In panels (d-e), even more abrupt jumps than the previous ones are observed, with a back-and-forth dynamics, with characteristic jump times of about 300 sec. Finally, in panel (f), a much faster back-and-forth dynamics is observed, so that the time of permanence in a state is of the order of 20 s. It is important to note that for long times the average y-displacement should be zero, since there is no symmetry breaking on the y-axis, so the apparent jump in the position of the panels (a-c) should eventually return close to its original position if we wait long enough. We believe that the abrupt jumps observed in figure 3.15 are due to fluctuations in the bacterial flux, so that movement occurs when the collective movement of the bacteria is sufficiently large, and this can vary from drop to drop, as shown in figure 3.8. It is also possible that the droplet sometimes pins to the surface, preventing it from moving in either direction.

Few results of rectification in the x-direction were obtained, one of which is shown in Figure 3.13. Panel (a) shows 2 snapshots of a TBM whose density and radius are given, respectively, by $n \sim 9.8 \times 10^8$bact/mL and $r = 30\,\mu$m, sitting on a ratchet-type surface. Panel (b) shows the trajectory of this TBM as a function of time. It can be seen that at a given time, rectification occurs in the expected x-axis. Note that there is also a slight displacement in the y-direction at the moment of rectification. This is due to the fact that at the moment of rectification the TBM traction increases and, being a random particle, it can move in any direction according to the internal fluctuations of the TBM generated by the micro-swimmers.

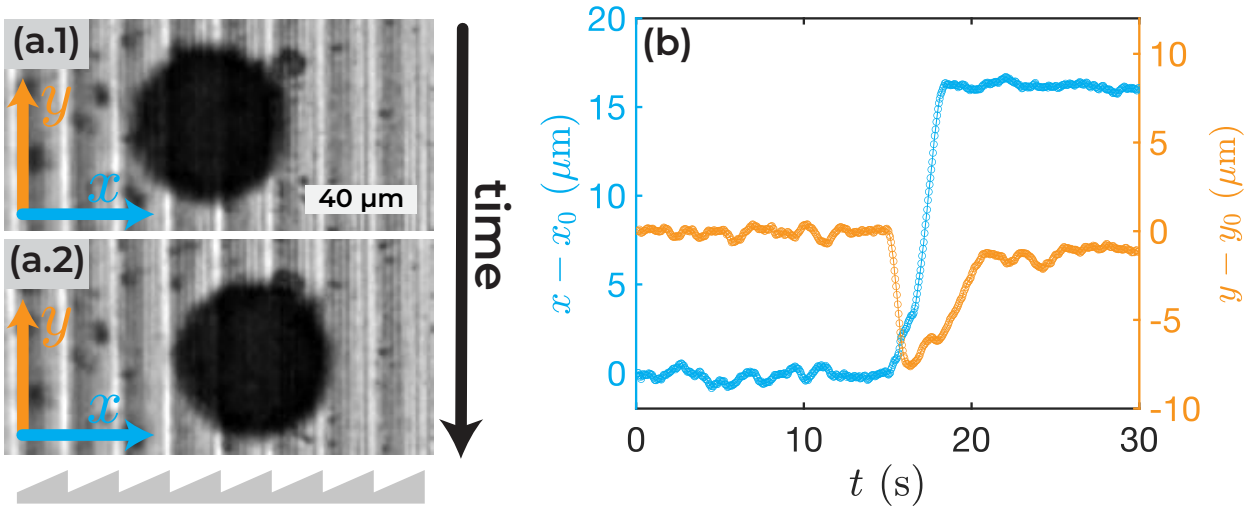

Figure 3.13: a) 2 snapshots of a TBM with density $n \sim 9.8 \times 10^8$bact/mL and radius $r = 30\,\mu$m resting on a ratchet-type surface. It can see how the TBM jumps from one well to another. The ratchet direction is shown at the bottom of the screen. (b) Trajectory of the TBM showing the jump on the x-axis.

One way to understand this behavior is to think of each staircase as a potential well for the TBM. In this sense, a weaker, i.e. shallower, potential well is required for the energy of the TBM to make it jump from one potential well to the next. In the same sense, this is what is observed in figure 3.13. With the same understanding, it can be intuited that the

TBM will continue to move along the y-axis if it is unable to jump between potential wells on the x-axis.

3.3.3 Ratchet-type channels

An alternative way to break the spatial symmetry is to create channels whose walls are not smooth, but rather ratchet-like. The result of this technique is channels with very precisely patterned walls. The schematic idea and a result of this is shown in figure 3.14. Attempts

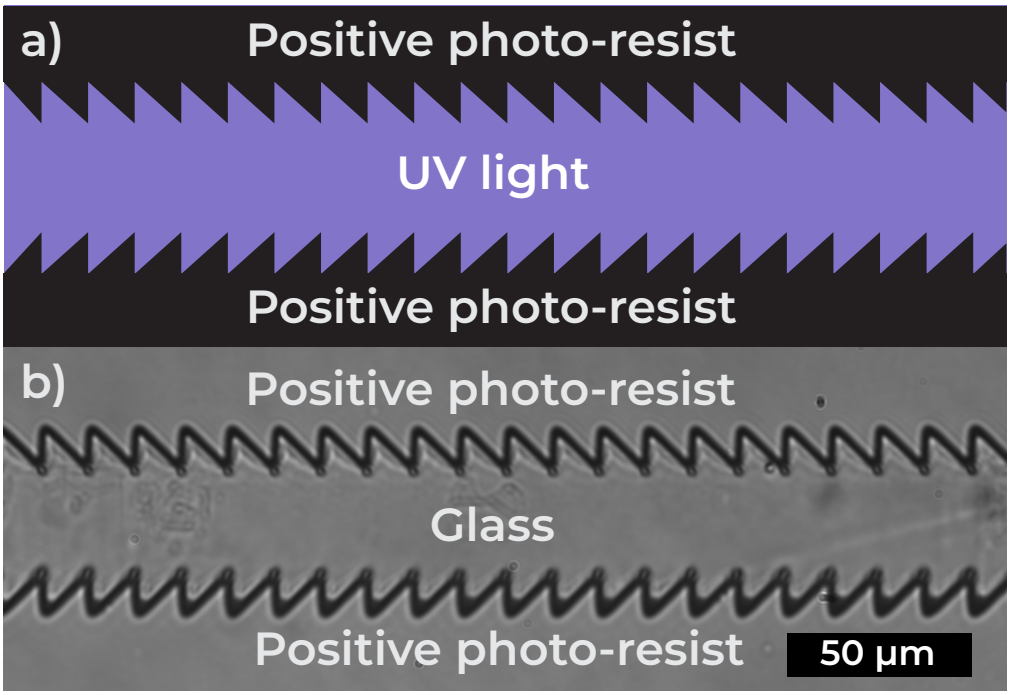

Figure 3.14: a) Design schematics and b) results of the micro-fabrication with positive photo-resist for the ratchet-type channels.

have been made to place TBMs on these channels and what has been systematically observed is that the TBMs get stuck without being able to move forward. This is most likely due to the irregularity of the ratchet tips causing the drop to get pinned. Figure 3.15 shows a snapshot of a TBM inside a ratchet-type channel. This remains in the same position throughout the video.

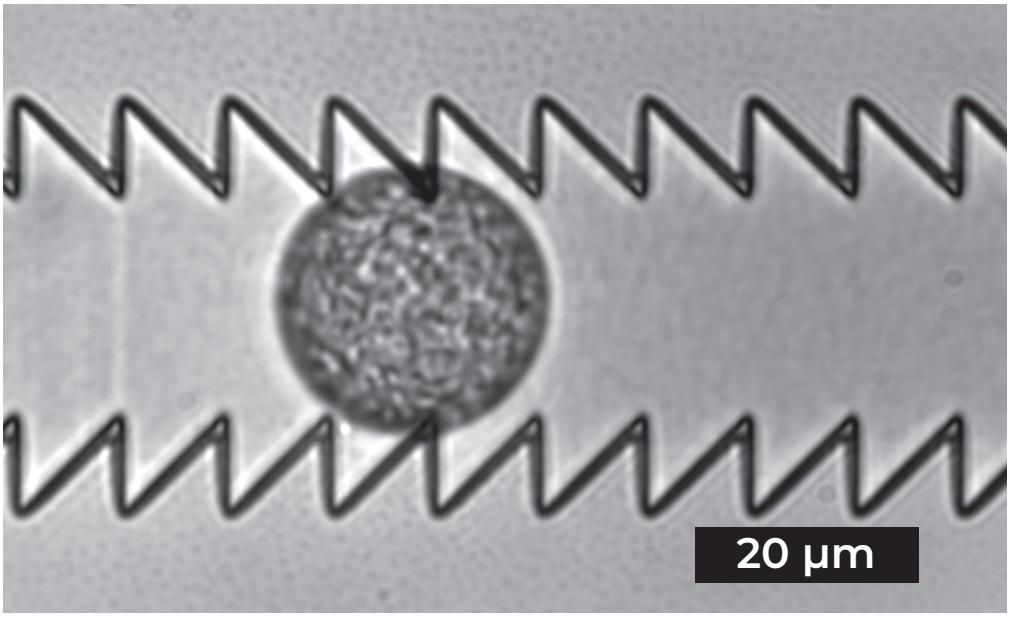

Figure 3.15: TBM in a channel with ratchet walls.

Chapter 4

Conclusions and perspectives

In this thesis, exploratory studies were conducted in three configurations of dense and highly confined bacterial baths. First we studied a quasi-2D flat confinement, which we call active carpets, then a spherical confinement, which we call active drops, and finally transnational bacterial motors (TBMs), which consists of an active drop that is able to self-propel. This chapter presents the main conclusions that have been obtained in this thesis for the three configurations that have been studied and the perspectives for each of them.

In the case of active carpets, it was found that the diffusion coefficient D and the persistence velocity v increase with the radius r of the passive particle driven by the active carpet. We believe this is due to the fact that by increasing the radius r of the passive particle, it has more surface area to be propelled by the coherent flows generated by the bacteria in the active carpet. On the other hand, the diffusion time τ has no clear dependence on the passive particle radius r. We believe this is because this time is related to the persistence time of the flow generated by the bacterial bath, which depends on the density and type of bacteria in the bath, but not the radius r of the passive particle.

As a perspective to the active carpet experiment, systematic experiments should be performed varying the carpet density to observe the density dependence of the D, v and τ parameters. In addition, it would be interesting to see how the behavior of the bacterial bath changes when it consists of *B. subtilis* bacteria instead of *E. coli*. On the other hand, it would be useful to measure the velocity field generated by the bacteria in the active carpet and decompose it into POD modes, as was done for the active droplets. This analysis could give us a different insight on the bacterial bath. Finally, measuring the correlation of passive particle pairs could give us significant insight into the characterization of active carpets.

In the case of active droplets, it was observed that in both *E. coli* and *B. subtilis* droplets, many modes are needed to have all the information of the velocity field, hence the similarity with the characteristic flows of inertial turbulence. Moreover, in both cases the predominant mode corresponds to a rotating vortex. In the case of the *E. coli* droplet, it was observed that the velocity field of the modes must be homogeneous in space, while in the *B. subtilis* droplets the activity, i.e.,the velocity field, is more intense at the edges of the droplet. We believe that this behavior is due in part to the elongated aspect ratio of *B. subtilis* bacteria relative to *E. coli*, which makes *B. subtilis* tend to align with walls and interfaces. The

most important result is that we observed for the first time edge modes in a spherical confinement configuration, confirming the phenomenology reported for rectangular confinement [Henshaw et al., 2023], where the size of the dominant structures is much larger than the size of the individual swimmers.

As a perspective for the active droplet experiment, a systematic study of the behavior of the POD modes as a function of the density of the bacterial bath should be made. It is possible that the configuration of the POD modes will be very different when the density is drastically varied. It would also be interesting to see if the same mode configuration is maintained when the droplet radius is increased significantly.

In the TBMs experiment, it was observed that there is a large scatter in D, v and τ as a function of the passive particle radius r, as reported in the literature [Ramos et al., 2020]. Unlike the active carpets, there is no clear dependence in any of the parameters with the radius of the active droplet r. It is observed that the values of D and v are generally lower than those observed for active particles driven by the active carpet, while the persistence time τ has values in a similar range. The latter contributes to the belief that the parameter τ has a close relationship with the persistence time of the flow generated by the bacterial bath. Regarding the rectification of the motion of TBMs, it was observed that ratchet-type substrates are an interesting system to study rectification. When the energy of the TBM is not high enough, it is unable to jump from one 'potential well' to another and remains in Brownian motion in a direction perpendicular to the asymmetry of the ratchet. When the energy is sufficient, we have observed that it is capable of jumping from one 'potential well' to the next, discretely rectifying its motion. We found that ratchet-type channels were not an efficient method for TBM rectification.

As a perspective, it is necessary to look for a substrate that prevents the TBMs from pinning to the surface, this would promote the movement of the TBMs, making rectification more likely. An interesting way to measure the efficiency of rectification on ratchet-type substrates is to induce flow in the asymmetric direction. One way to do this is to tilt the substrate in both directions and, after repeating the experiment many times, determine which way the TBM jumps more often. By having more TBM jumps from one 'potential well' to another, one can measure a residence time in each well, which is likely to be different for each direction of the ratchet.

Bibliography

[men, 2023] (2023). *Data-Driven Fluid Mechanics: Combining First Principles and Machine Learning*. Cambridge University Press.

[Balda et al., 2022] Balda, A. B., Argun, A., Callegari, A., and Volpe, G. (2022). Playing with active matter.

[Bartussek et al., 1996] Bartussek, R., Reimann, P., and Hänggi, P. (1996). Precise numerics versus theory for correlation ratchets. *Phys. Rev. Lett.*, 76:1166–1169.

[Bechinger et al., 2016] Bechinger, C., Leonardo, R. D., Löwen, H., Reichhardt, C., Volpe, G., and Volpe, G. (2016). Active particles in complex and crowded environments. *Reviews of Modern Physics*, 88(4).

[Das et al., 2020] Das, M., Schmidt, C. F., and Murrell, M. (2020). Introduction to active matter. *Soft Matter*, 16:7185–7190.

[DiLuzio et al., 2005] DiLuzio, W. R., Turner, L., Mayer, M., Garstecki, P., Weibel, D. B., Berg, H. C., and Whitesides, G. M. (2005). Escherichia coli swim on the right-hand side. *Nature*, 435(7046):1271–1274.

[Drescher et al., 2011] Drescher, K., Dunkel, J., Cisneros, L. H., Ganguly, S., and Goldstein, R. E. (2011). Fluid dynamics and noise in bacterial cell–cell and cell–surface scattering. *Proceedings of the National Academy of Sciences*, 108(27):10940–10945.

[Dubay et al., 2022] Dubay, M. M., Johnston, N., Wronkiewicz, M., Lee, J., Lindensmith, C. A., and Nadeau, J. L. (2022). Quantification of motility in bacillus subtilis at temperatures up to 84°c using a submersible volumetric microscope and automated tracking. *Frontiers in Microbiology*, 13.

[Fox, 1998] Fox, R. F. (1998). Rectified brownian movement in molecular and cell biology. *Phys. Rev. E*, 57:2177–2203.

[Gachelin et al., 2014] Gachelin, J., Rousselet, A., Lindner, A., and Clement, E. (2014). Collective motion in an active suspension of escherichia coli bacteria. *New Journal of Physics*, 16(2):025003.

[Grognot and Taute, 2021] Grognot, M. and Taute, K. M. (2021). More than propellers: how flagella shape bacterial motility behaviors. *Current Opinion in Microbiology*, 61:73–81.

[Guzmán-Lastra et al., 2021] Guzmán-Lastra, F., Löwen, H., and Mathijssen, A. J. T. M. (2021). Active carpets drive non-equilibrium diffusion and enhanced molecular fluxes. *Nature Communications*, 12(1):1906.

[Henshaw et al., 2023] Henshaw, R. J., Martin, O. G., and Guasto, J. S. (2023). Dynamic mode structure of active turbulence. *Phys. Rev. Fluids*, 8:023101.

[Hu et al., 2015] Hu, J., Yang, M., Gompper, G., and Winkler, R. G. (2015). Modelling the mechanics and hydrodynamics of swimming e. coli. *Soft Matter*, 11:7867–7876.

[Kim and Breuer, 2008] Kim, M. J. and Breuer, K. S. (2008). Microfluidic pump powered by self-organizing bacteria. *Small*, 4(1):111–118.

[Lauga et al., 2006] Lauga, E., DiLuzio, W. R., Whitesides, G. M., and Stone, H. A. (2006). Swimming in circles: Motion of bacteria near solid boundaries. *Biophysical Journal*, 90(2):400–412.

[Leonardo et al., 2010] Leonardo, R. D., Angelani, L., Dell'Arciprete, D., Ruocco, G., Iebba, V., Schippa, S., Conte, M. P., Mecarini, F., Angelis, F. D., and Fabrizio, E. D. (2010). Bacterial ratchet motors. *Proceedings of the National Academy of Sciences*, 107(21):9541–9545.

[Malgaretti et al., 2012] Malgaretti, P., Pagonabarraga, I., and Rubí, J. M. (2012). Cooperative rectification in confined brownian ratchets. *Phys. Rev. E*, 85:010105.

[Martens et al., 2012] Martens, K., Angelani, L., Di Leonardo, R., and Bocquet, L. (2012). Probability distributions for the run-and-tumble bacterial dynamics: An analogy to the lorentz model. *The European Physical Journal E*, 35(9):84.

[Patteson et al., 2016] Patteson, A. E., Gopinath, A., Purohit, P. K., and Arratia, P. E. (2016). Particle diffusion in active fluids is non-monotonic in size. *Soft Matter*, 12:2365–2372.

[Porvatov et al., 2021] Porvatov, V. A., Rozenblit, A. D., Dmitriev, A. A., Burmistrov, O. I., Petrova, D. A., Gritsenko, G. Y., Puhtina, E. M., Kretov, E. I., Filonov, D. S., Souslov, A., and Olekhno, N. A. (2021). Optimizing self-rotating bristle-bots for active matter implementation with robotic swarms. *Journal of Physics: Conference Series*, 2086(1):012202.

[Purcell, 1977] Purcell, E. M. (1977). Life at low Reynolds number. *American Journal of Physics*, 45(1):3–11.

[Ramos et al., 2020] Ramos, G., Cordero, M. L., and Soto, R. (2020). Bacteria driving droplets. *Soft Matter*, 16:1359–1365.

[Sipos et al., 2015] Sipos, O., Nagy, K., Di Leonardo, R., and Galajda, P. (2015). Hydrodynamic trapping of swimming bacteria by convex walls. *Phys. Rev. Lett.*, 114:258104.

[Sokolov et al., 2010] Sokolov, A., Apodaca, M. M., Grzybowski, B. A., and Aranson, I. S. (2010). Swimming bacteria power microscopic gears. *Proceedings of the National Academy of Sciences*, 107(3):969–974.

[Sokolov and Aranson, 2012] Sokolov, A. and Aranson, I. S. (2012). Physical properties of collective motion in suspensions of bacteria. *Phys. Rev. Lett.*, 109:248109.

[Tapia-Ignacio et al., 2021] Tapia-Ignacio, C., Gutierrez-Martinez, L. L., and Sandoval, M. (2021). Trapped active toy robots: theory and experiment. *Journal of Statistical Mechanics: Theory and Experiment*, 2021(5):053404.

[Vicsek et al., 1995] Vicsek, T., Czirók, A., Ben-Jacob, E., Cohen, I., and Shochet, O. (1995). Novel type of phase transition in a system of self-driven particles. *Phys. Rev. Lett.*, 75:1226–1229.

[Wensink et al., 2012] Wensink, H. H., Dunkel, J., Heidenreich, S., Drescher, K., Goldstein, R. E., Löwen, H., and Yeomans, J. M. (2012). Meso-scale turbulence in living fluids. *Proceedings of the National Academy of Sciences*, 109(36):14308–14313.

[Wioland et al., 2013] Wioland, H., Woodhouse, F. G., Dunkel, J., Kessler, J. O., and Goldstein, R. E. (2013). Confinement stabilizes a bacterial suspension into a spiral vortex. *Phys. Rev. Lett.*, 110:268102.

[Wu and Libchaber, 2000] Wu, X.-L. and Libchaber, A. (2000). Particle diffusion in a quasi-two-dimensional bacterial bath. *Phys. Rev. Lett.*, 84:3017–3020.

[Zhang et al., 2021] Zhang, B., Leishangthem, P., Ding, Y., and Xu, X. (2021). An effective and efficient model of the near-field hydrodynamic interactions for active suspensions of bacteria. *Proceedings of the National Academy of Sciences*, 118(28):e2100145118.